FINAL REPORT

Continuous Monitoring of Mobility, Burial and Re-exposure of Underwater Munitions in Energetic Near-Shore Environments

SERDP Project MR-2319

JANUARY 2017

Peter Traykovski
Thomas Austin
Woods Hole Oceanographic Institution

Distribution Statement A
This document has been cleared for public release

SERDP
DOD ▪ EPA ▪ DOE

Page Intentionally Left Blank

This report was prepared under contract to the Department of Defense Strategic Environmental Research and Development Program (SERDP). The publication of this report does not indicate endorsement by the Department of Defense, nor should the contents be construed as reflecting the official policy or position of the Department of Defense. Reference herein to any specific commercial product, process, or service by trade name, trademark, manufacturer, or otherwise, does not necessarily constitute or imply its endorsement, recommendation, or favoring by the Department of Defense.

Page Intentionally Left Blank

REPORT DOCUMENTATION PAGE

Form Approved
OMB No. 0704-0188

Public reporting burden for this collection of information is estimated to average 1 hour per response, including the time for reviewing instructions, searching existing data sources, gathering and maintaining the data needed, and completing and reviewing this collection of information. Send comments regarding this burden estimate or any other aspect of this collection of information, including suggestions for reducing this burden to Department of Defense, Washington Headquarters Services, Directorate for Information Operations and Reports (0704-0188), 1215 Jefferson Davis Highway, Suite 1204, Arlington, VA 22202-4302. Respondents should be aware that notwithstanding any other provision of law, no person shall be subject to any penalty for failing to comply with a collection of information if it does not display a currently valid OMB control number. **PLEASE DO NOT RETURN YOUR FORM TO THE ABOVE ADDRESS.**

1. REPORT DATE *(DD-MM-YYYY)*
08-17-2016

2. REPORT TYPE
Final Report

3. DATES COVERED *(From - To)*
5/2013-09/2016

4. TITLE AND SUBTITLE
Continuous Monitoring of Mobility, Burial, and Re-exposure of Underwater Munitions in Energetic Near-Shore Environments

5a. CONTRACT NUMBER
W912HQ-13-C-0044

5b. GRANT NUMBER

5c. PROGRAM ELEMENT NUMBER

6. AUTHOR(S)
P. Traykovski
T. Austin

5d. PROJECT NUMBER

5e. TASK NUMBER

5f. WORK UNIT NUMBER

7. PERFORMING ORGANIZATION NAME(S) AND ADDRESS(ES)
Woods Hole Oceanographic Institution
266 Woods Hole Road
Woods Hole, MA 02543

8. PERFORMING ORGANIZATION REPORT NUMBER

9. SPONSORING / MONITORING AGENCY NAME(S) AND ADDRESS(ES)
Strategic Environmental Research and Development Program
4800 Mark Center Dr, Ste 17D08
Alexandria, VA 22350

10. SPONSOR/MONITOR'S ACRONYM(S)
SERDP

11. SPONSOR/MONITOR'S REPORT NUMBER(S)
MR-2319

12. DISTRIBUTION / AVAILABILITY STATEMENT

13. SUPPLEMENTARY NOTES

14. ABSTRACT
The development of predictive models and measurement techniques for the mobility, burial, and reexposure of munitions is essential to planning remediation efforts. In sandy, energetic, nearshore environments, the migration, burial, and reexposure processes all have the potential to be active depending on munition properties and forcing parameters. The goal of this work was to develop technology for surveying small-scale seafloor morphology and bathymetry, determining the location and state of burial of active Unexploded Ordnance (UXO) surrogates with imbedded acoustic transponders, and conducting field measurements that span the relevant parameter space at the transition from burial to mobility. To further our understanding of UXO burial and mobility processes, a range of different size and density active UXO surrogates were deployed in energetic surf zone and tidal shoal environments. These deployments and surveys filled gaps in our knowledge in parts of parameter space conducive to high munition mobility (energetic conditions, rapidly changing bathymetry, and a range of UXO densities) that have not been adequately sampled by previous field efforts

15. SUBJECT TERMS

16. SECURITY CLASSIFICATION OF:

a. REPORT	b. ABSTRACT	c. THIS PAGE
UU	UU	UU

17. LIMITATION OF ABSTRACT
UU

18. NUMBER OF PAGES
44

19a. NAME OF RESPONSIBLE PERSON
Peter Traykovski

19b. TELEPHONE NUMBER *(include area code)*
508-289-2638

Standard Form 298 (Rev. 8-98)
Prescribed by ANSI Std. Z39.18

Page Intentionally Left Blank

Table of Contents

List of Figures 3
Acronyms 5
Abstract 6
1. Objectives 8
1.1. SERDP Relevance 8
2. Background 8
2.1. Theory 9
2.1.1. Object Mobility 9
2.1.2. Object Burial 11
2.2. Previous Measurements 11
3. Materials and Methods 12
3.1. Location Study Sites 12
3.2. UXO Surrogate Objects 14
3.2.1. GPS and Passive Buoys 14
3.2.2. Embedded Motion Sensors 15
3.2.3. Acoustic Tracking Systems 15
3.3. Bathymetric Mapping Techniques 16
3.3.1. Wasque Shoals Bathymetry 17
3.3.2. Long Point Surf Zone Bathymetry 18
3.4. Measurement Techniques for Forcing Hydrodynamics and Small-Scale Bedforms 18
4. Results and Discussion 21
4.1. Wasque Tidal Shoals 21
4.1.1. Hydrodynamic Forcing 21
4.1.2. Small-Scale Bedforms 23
4.1.3. UXO Surrogate Deployments 24
4.2. Long Point Surf Zone 28
4.2.1. Hydrodynamic Forcing 29
4.2.2. Small-Scale Bedforms 30
4.2.3. UXO Surrogate Deployments 31
4.3. Discussion of Theory and Hydrodynamic Forcing 34
4.3.1. Hydrodynamic Modeling 34
4.3.2. Comparison to Parameterized Models 35
5. Conclusions and Implications for Future Research/Implementation 37
6. Literature Cited 39
7. Appendices 41

List of Figures

Figure 1. Parameterized forces on a partially buried cylinder 9
Figure 2. Threshold for initiation of motion as a function of UXO density and wave forcing 10
Figure 3. Location of study site and Cape Cod regional bathymetry, with aerial imagery of Wasque Shoals, and sidescan sonar imagery of the area near Martha's Vineyard Coastal Observatory (MVCO) 12
Figure 4. UXO (1) and notices to public at Long Point, MV 13
Figure 5. MVCO wave height statistics 13
Figure 7. a) Passive tracking buoys and b) GPS tracking buoy 14
Figure 6. Surrogate UXO 14
Figure 8. IMU mounted on the endcap of the pressure case inside a surrogate UXO 15
Figure 9. USBL array (left) and interrogation transponder (right) 15
Figure 11. Jetyak surveying at (a) Wasque Shoals and (b) Long Point 16
Figure 10. Schematic of Jetyak ASV System 16
Figure 12. Bathymetry of Wasque Shoals in Oct. 2013, Jan. 2014, and July 2014, showing the migration of a large dune over our instrumented quadpod (location indicated by triangle)..... 17
Figure 13. Long Point surf zone site bathymetry 18
Figure 14. Schematic of (a) a quadpod and (b) pole mount sensors 19
Figure 16. Quadpod and instruments at Long Point 20
Figure 15. Quadpod and instruments at Wasque Shoals 20
Figure 17. Time series of downward-aimed acoustic backscatter and hydrodynamic sensors from Wasque Shoals 21
Figure 18 Time series of wave parameters on Wasque Shoals 22
Figure 19. Rotary sonar imagery showing migrating mega-ripples and the beginning (a) green transect in (c) and end (b) yellow transect in (c) of a three-day period. Sidescan backscattered intensity along the transect shown by the green and yellow lines reveals the convergence and divergence of the migrating mega-ripples. 23
Figure 20. (a) Location of GPS buoy-tracked UXO at Wasque Shoals relative to quadpod and time series of (b) light and (c) medium density GPS buoy-tracked UXO locations..... 24
Figure 21. Time series of hydrodynamic and migrating bedform forcing and UXO mobility based on IMU data from Wasque Shoals 25
Figure 22. Migration paths of light and medium surrogate UXO superimposed on bathymetry (a) before the beginning of the depoyment and (b) at the recovery 26
Figure 23. Scatter plot of UXO roll r.m.s. variations (indicated by size of symbol) vs. current and wave velocity 26
Figure 24. Succesive rotary sonar images showing transient burial and reexposure of a surrogate UXO by migrating mega-ripples at Wasque Shoals 27
Figure 25. Time series of hydrodynamic forcing (upper panels) and USBL range and bearing (lower panel) 28
Figure 26. Time series of wave parameters at Long Point 29
Figure 27. (a) Rotary sonar imagery and (b) Jetyak-based sidescan imagery of wave orbital scale ripples at Long Point 30
Figure 28. Bathymetry of Long Point surf zone and surrogate UXO trajectories 31
Figure 29. Distribution of stationary and mobile UXO vs. depth, density, and across-shore distance 32

Figure 30. UXO relative burial depth vs. relative density (S_0) with physical burial depth (m) in text. Large symbols are D_0 = 14 cm objects, and small symbols are D_0 = 7 cm objects. 33
Figure 31. (a) Snapshot of SWASH output showing wave shoaling transformation, and (b) interpolation of wave orbital velocities from the sensor location to the UXO deployment location 34
Figure 32. Time series of UXO r.m.s. roll variations and wave orbital velocity..... 35
Figure 33 (a) Threshold for initiation of UXO motion as a function of U_{br} and S_o based on asumed initial burial of 10% and 30%. (b) Threshold for initiation of motion based on an equilibrium burial depth assumption. 36
Figure 34. Threshold for initiation of UXO motion as a function of U_{br} and S_o based on a time-dependent burial fomulation with four different choices of the rate of wave velcoity change (dU_{br}/dt)..... 37

Acronyms

ABS	Acoustic Backscatter Sensor
ADV	Acoustic Doppler Velocimeter
ASV	Autonomous Surface Vessel
AWAC	Acoustic Wave And Current
CFD	Computational Fluid Dynamics
CONUS	Contiguous United States
CORS	Continuously Operating Reference Station
COTS	Commercial Off The Shelf
DH	Deep-Heavy
DL	Deep-Light
ESTCP	Environmental Security Technology Certification Program
FY	Fiscal Year
GPS	Global Positioning System
IMU	Inertial Motion Unit
MBP	Mine Burial Program
MEMS	Microelectromechanical Systems
MIT	Massachusetts Institute of Technology
MM	Munition Mobility
MRSON	Munitions Response Statement of Need
MVCO	Martha's Vineyard Coastal Observatory
NAD	North American Datum
NAVD	North American Vertical Datum
ONR	Office of Naval Research
PCDP	Pulse-Coherent Doppler Profiler
PPK	Post-Processed Kinetic
RC	Remote Control
REMUS	Remote Environmental Monitoring Underwater System
RTK	Real-Time Kinetic
sdl	small-diameter-light
sdm	small-diameter-medium
SERDP	Strategic Environmental Research and Development Program
SL	Shallow-Light
SNR	Signal-to-Noise Ratio
SWASH	Simulating WAves till SHore
TRIADS	Non-Linear Wave Triad Interaction Model
UnMES	Underwater Munitions Expert System
USBL	Ultra-Short Base Line
UXO	Unexploded Ordnance
WBH	Wasque-Buoy-Heavy
WBL	Wasque-Buoy-Light
WBM	Wasque-Buoy-Medium
WHOI	Woods Hole Oceanographic Institution

Abstract

Objectives: The development of predictive models and measurement techniques for the mobility, burial, and reexposure of munitions is essential to planning remediation efforts. In sandy, energetic, nearshore environments, the migration, burial, and reexposure processes all have the potential to be active depending on munition properties and forcing parameters. The goal of this work was to develop technology for surveying small-scale seafloor morphology and bathymetry, determining the location and state of burial of active Unexploded Ordnance (UXO) surrogates with imbedded acoustic transponders, and conducting field measurements that span the relevant parameter space at the transition from burial to mobility. To further our understanding of UXO burial and mobility processes, a range of different size and density active UXO surrogates were deployed in energetic surf zone and tidal shoal environments. These deployments and surveys filled gaps in our knowledge in parts of parameter space conducive to high munition mobility (energetic conditions, rapidly changing bathymetry, and a range of UXO densities) that have not been adequately sampled by previous field efforts.

Technical approach: The analysis and field measurement program was guided by a parameterized force balance model for the mobility and burial of UXO in sandy sediments. Based on this force balance, surrogate UXO with relative densities significantly above the density of water, but both above and below the bulk density of water-saturated sand, were chosen to ensure that some objects would be mobile and others would bury. The measurements included in situ continuous monitoring of processes via seafloor frame-mounted rotary sidescan sonars and water velocity sensors, an Ultra-Short Base Line (USBL) acoustic tracking system, Global Positioning System (GPS) buoy-based tracking, and manual passive buoy-based tracking. Measurements were conducted both on Wasque Shoals, near the Muskeget tidal channel between Martha's Vineyard and Nantucket, MA, and at the Long Point, Martha's Vineyard surf zone site with weaker tidal currents. Despite both sites having similar wave forcing conditions, the large dunes at the tidally forced site severely constrained UXO migration. Surrogate UXO with relative densities less than water-saturated sand migrated a maximum distance of 14 m, as the objects migrated into the troughs of the large dunes (100 m wavelength, 3 m height). At the surf zone site, UXO surrogates with relative densities less than water-saturated sand migrated 100 to 150 m onshore, came to rest, and subsequently buried 40 m from the beach. Objects with relative densities that were significantly higher than water-saturated sand tended to bury at their deployment location. No objects migrated into the nearshore swash zone or onto the beach as waves breaking offshore decreased the nearbed wave orbital velocity within 50 m of the beach. Predictions of mobility, based on parameterized force balances with a constant initial burial of 10% or 30% of the object diameter, could *not* predict the measured transition from burial to mobility as a function of wave orbital velocity and UXO relative density. Calculations based on 10% initial burial incorrectly predicted that all objects in the measured data set would be mobile, and calculations based on 30% initial burial incorrectly predicted that all objects in the measured data set would be stationary and buried. Time-dependent calculations that account for the time required for burial of an object were able to successfully predict the initiation of mobility consistent with the observations. In these calculations, the timescale for burial is set by the ratio of the burial scour pit cross-sectional area relative to the sediment transport rate. If the waves increase quickly enough that an object does not have time to bury before the threshold for mobility is reached, it will migrate. If the waves increase slowly, these calculations predict that even low-density objects will bury.

Benefits: The measurements conducted in this study provide a unique data set on munitions burial, reexposure, and migration in energetic nearshore conditions where the potential for significant migration is high. We now have knowledge on the parameters required for moderate distance (100 m) migration that was not previously available. This study provides data on the behavior of a range of different density objects in energetic conditions with mobile nearshore bathymetry to better span parameter space for the development of deterministic predictive models. These deterministic models can be used as input to statistical models for operation over longer time periods and larger spatial domains with greater uncertainty in forcing conditions. An important conclusion from this study is that the time history of the forcing can determine the relative roles of processes causing burial or mobility, which needs to be accounted for in deterministic and statistical models. The technology development of USBL tracking provides a means for tracking objects in energetic conditions that can be used in future studies of munition mobility and burial.

1. Objectives

The development of predictive models for the mobility, burial, and reexposure of munitions is essential to planning remediation efforts. In sandy, energetic nearshore environments, the migration, burial and reexposure processes all have the potential to be active depending on the munition properties and forcing parameters. The parameter space in which objects migrate significant distances has not been thoroughly examined with quantitative field measurements. To obtain data to quantify these processes and test models, we conducted field measurements of mobility, burial, and reexposure of munitions in energetic nearshore environments with a high potential for mobility. The surrogate munition's type, size, and density were varied to enhance the potential for migration processes. An autonomous four-transducer USBL transceiver system was developed to continuously track objects during energetic conditions. The system acoustically measured range and bearing to surrogate munitions equipped with acoustic transponders. The measurements were examined to understand munition mobility and burial processes, as well as to develop relations between these processes and bedform geometry, migration, and hydrodynamic forcing. Finally, simple parameterized models were examined and refined in the parameter space consistent with the observations.

1.1. SERDP Relevance

One of the areas outlined in the Strategic Environmental Research and Development Program (SERDP) munitions response program area statement of need for FY 2013 was the characteristics of underwater munitions and their environment. This includes "assessing and predicting the locations of munitions relative to the seafloor: whether they are found proud on the sea bottom, partially buried, or completely buried in the sediment as a function of historical use and site conditions." The migration and burial of munitions is closely linked to sediment type, seafloor morphology, and hydrodynamic conditions, as migrating bedforms may bury munitions, and munitions may potentially migrate with the bedforms. Migration of munitions is a challenge for remediation efforts because objects can migrate into areas that have been previously cleared, or objects that have been detected and located either can migrate or become buried before removal. An increased ability to predict burial and migration processes has the potential to ensure that appropriate decisions are made in the timing, scope, and duration of remediation efforts.

2. Background

Although a considerable amount of work has been conducted to measure the mobility, burial, and reexposure of munitions and in developing predictive models, significant gaps still remain in our knowledge of these processes. The part of parameter space where significant (greater than 10 to 30 m) migration occurs has not been thoroughly examined. In addition, very few continuous measurements have been made of mobility, burial, and reexposure of munitions because most measurements have been conducted by diver surveys or by using acoustic transponders and a transceiver deployed on a small boat, which measures the state of the munitions before and after—but not during—the energetic conditions that cause mobility and burial. To our knowledge, prior to the present study, autonomous, self-contained data-logging USBL systems that could be used to continuously track mobile objects were not commercially available.

During the Office of Naval Research Mine Burial Prediction Program (ONR-MBP), several technologies were developed at Woods Hole Oceanographic Institution (WHOI) to provide

continuous data on the state of burial of large (approximately 50 cm diameter by 1.5 m long) mine-shaped objects, with a relative submerged density ($S_o = \rho_o/\rho_w$) of 2.4, where ρ_o is the density of the object, and ρ_w is the density of water (2, 3, 4). Rotary sidescan sonars were mounted on fixed frames adjacent to the mobile mine-shaped objects. The imagery from these sonars revealed no migration, complete burial in fine sand (d_{50} = 180 μm), and partial burial in coarse sand (d_{50} = 650 μm) during the same hydrodynamic forcing conditions. The rotary sonars combined with sensors integrated into the mines provided a unique data set with two distinct points in the grain size parameter space, which was used to improve mine burial prediction models. Due to the large size, relative density, and moderate energy-forcing conditions in 12 m deep water, these objects were not expected to migrate significant distances, and the expected burial mechanism of scour and fill was consistent with the observations. The horizontal motion of the objects was limited to less than 1 m as the mines rolled into their own scour pits in fine sand or rotated to align with wave-formed bedforms in coarse sand.

2.1. **Theory**

2.1.1. Object Mobility

The parameter space where burial vs. migration is expected can be examined by considering the moments on an object and the grains of sand. In a highly simplified analysis, the moment per unit length that will induce roll of the cylinder is $F\ (D_o/2 - b_d)$, where D_o is the diameter of the object, and b_d is the depth of burial. The drag force due to water motion (F) is shown in (Figure 1). The stabilizing moment caused by the weight of the cylinder per unit length when the object is less than halfway buried is $W\sqrt{b_d(D_o - b_d)}$. The ratio of the destabilizing forces to the stabilizing forces is quantified by the object Shields parameter (θ_{op_b}) based on percent burial ($p_b = b_d/D_0$):

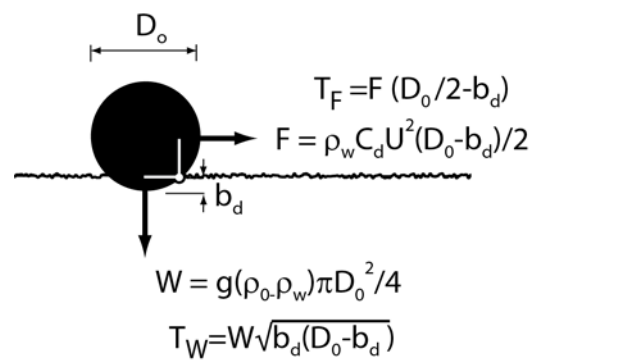

Figure 1. Parameterized forces on a partially buried cylinder

$$\theta_{op_b} = \frac{C_d U^2}{g(S_o - 1)D_0} \frac{(1 - p_b)^2}{\pi\sqrt{p_b(1 - p_b)}} = \theta_o \frac{(1 - p_b)^2}{\pi\sqrt{p_b(1 - p_b)}} \tag{1}$$

The key parameters in this expression are the diameter of the object and the initial depth of burial as these determine the moment arms, and the steady current velocity (U) combined with the relative density of the object (S_o) as these determine the forces. A similar analysis on a grain of sand with median diameter d_{50} results in the Shields criteria for initiation of sand motion (5). The Shields parameter based on percent burial (θ_{op_b}) can be expressed as the Shields parameter from sediment transport theory θ_o and an initial burial term.

A recent reanalysis of previously collected data with additional new laboratory data on the initiation of UXO motion was conducted by Rennie, Brandt, and Friedrichs (RBF16, 6). They propose a relationship whereby the object Shields parameter (θ_o) is modified by an inertial term that accounts for the effects of flow acceleration due to waves as

$$f_I = (1 + 16\pi^2(C_I/C_D)^2 KC^{-2})^{\frac{1}{2}} \tag{2}$$

where C_I/C_D is approximately 2 for cylinders, and the Keulegan–Carpenter number is defined as $KC = U_{br}T/D_0$. The variable U_{br} is the representative nearbed wave orbital velocity, and T is the peak wave period. Based on a fit to data, RBF16 found a power law relation between the modified Shields parameter and the initial depth of burial (b_d/D_0) of the form:

$$f_I\theta_o = 1.64\left(\frac{b_d}{D_0}\right)^{0.71} \tag{3}$$

This criterion for mobility is illustrated as a relation between critical velocity and object relative density (S_o) for several different initial burial depths in Figure 2. The threshold for initiation of sand mobility based on median diameter (D_{50}) of 400 μm is also shown. The threshold for initiation of sediment motion is calculated from

$$\theta_{sed} = \frac{f_w U_{br}^2}{g(S_o - 1)d_{50}} \tag{4}$$

where the wave friction factor is based on the expression from Nielsen (7), in which d_{50} is the median grain diameter of the sand:

$$f_w = \exp\left(5.5\left(\frac{12U_{br}T}{2\pi d_{50}}\right)^{-0.2} - 6.3\right) \tag{5}$$

In terms of migration rates, two alternative hypotheses are available. The first is that the migration rate can be described by a similar parameterized balance between rolling resistance and hydrodynamic forces on the object. A second alternative hypothesis is that bedform migration rates could be the upper bound for the mobility speed of dense objects because rolling resistance would increase dramatically if the object were to roll up the slope of a bedform. If this is the case, a large body of knowledge on bedform migration could be applied to the munition mobility problem.

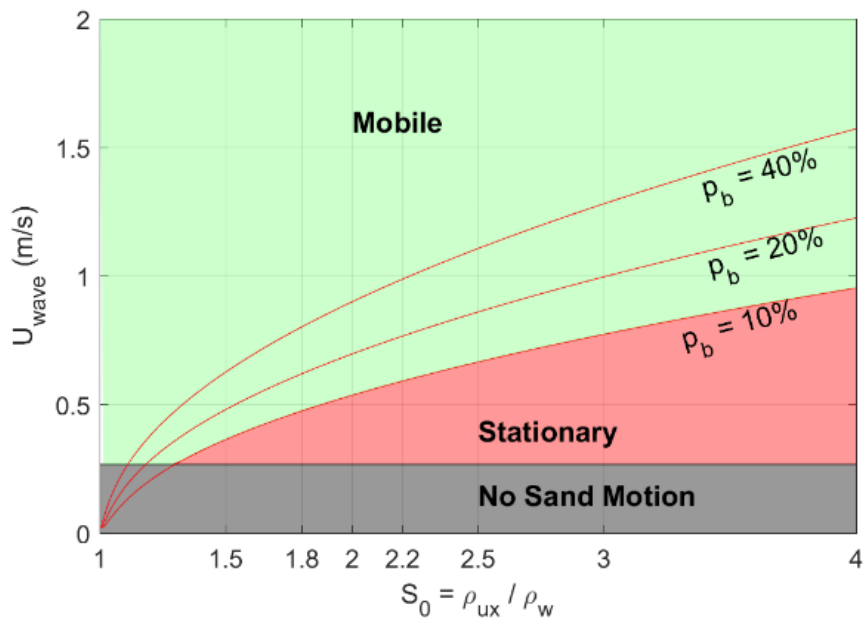

Figure 2. Threshold for initiation of motion as a function of UXO density and wave forcing

2.1.2. Object Burial

Laboratory data and some field data have also been used to develop parameterized expressions for the state of burial of cylinders, mines, and ordnance-shaped objects. Although there is a large body of literature on this subject, the results are well summarized in RBF2016 and a recent publication by Friedrichs, Rennie, and Brandt (8). This work suggests the following expression for equilibrium burial depth:

$$p_{b,eq} = a_2 \theta_{sed}^{b_2} \tag{6}$$

The values of Catano-Lopera et al. (9) of $a_2 = 1.6$ and $b_2 = 0.85$ for wave periods of T > 4 s were used for predictions of burial depth in this study. The equilibrium burial depth formulations relate the final depth of burial to constant wave forcing conditions. The burial process is known to take a finite amount of time, which is related to the sediment transport rate and the size of the scour pit that the object will self-bury in. Whitehouse (10) modeled time-dependent burial as a logistic process, whereby the burial depth (p_b) follows the equilibrium burial depth ($p_{b,eq}$) with a timescale (T^*):

$$\frac{dp_b}{dt} = \frac{p_{b,eq} - p_b}{T^*} \tag{7}$$

This expression is similar to that used by Traykovski (11) for modeling time-dependent evolution ripple geometry. For a step change in forcing, this results in the following:

$$p_b(t) = p_{b,eq}\left(1 - \exp\left(-\frac{t}{T^*}\right)\right) \tag{8}$$

The timescale is the ratio of the object diameter squared to the sediment transport rate:

$$T^* = \frac{M\theta_{sed}^N D_0^2}{(g(S_{sed} - 1)d_{50}^3)^{0.5}} \tag{9}$$

The parameter N is set to 1.5 based on the Meyer-Peter Mueller (12) sediment transport rate formulation, and M was set to 0.11 based on work by Demir and Garcia (13).

2.2. **Previous Measurements**

In addition to the laboratory measurements described in RBF2016, in order to validate a complex numerical model for UXO mobility, Jenkins (14, 15, 16) and colleagues both collected new data on object mobility and reexamined previously collect data. Their VORTEX Mobility Model (MM), which captures some of the three-dimensional complexity of the flow, was used in the ONR-MBP program and was subsequently used in SERDP/ Environmental Security Technology Certification Program (ESTCP) funded work to study both the migration and burial of 5”/38 and 20 mm shells (MR-0417 Field Deployment and MR-04017 Final Report). In those studies, objects were deployed both in a tropical reef nearshore environment at Kauai, Hawaii, and an energetic sandy beach environment at Duck, North Carolina. In the Kauai study, 5”/38 surrogate munitions with a relative density of 4.9 were deployed in a deep site in 16 m water depth and a shallow site in 8 m water depth and were exposed to waves that had heights of 0.5 to 1 m during most of the deployment with one event with $H_{sig} = 2$ m, $T = 12$ s waves. The predicted critical wave height for initiation of motion was 1.3 m at the shallow site and 1.7 m at the deep site. Due to the relatively calm conditions during the deployment, the relatively deep depth, and the high density of the objects, the waves were only slightly above the critical conditions for a few days,

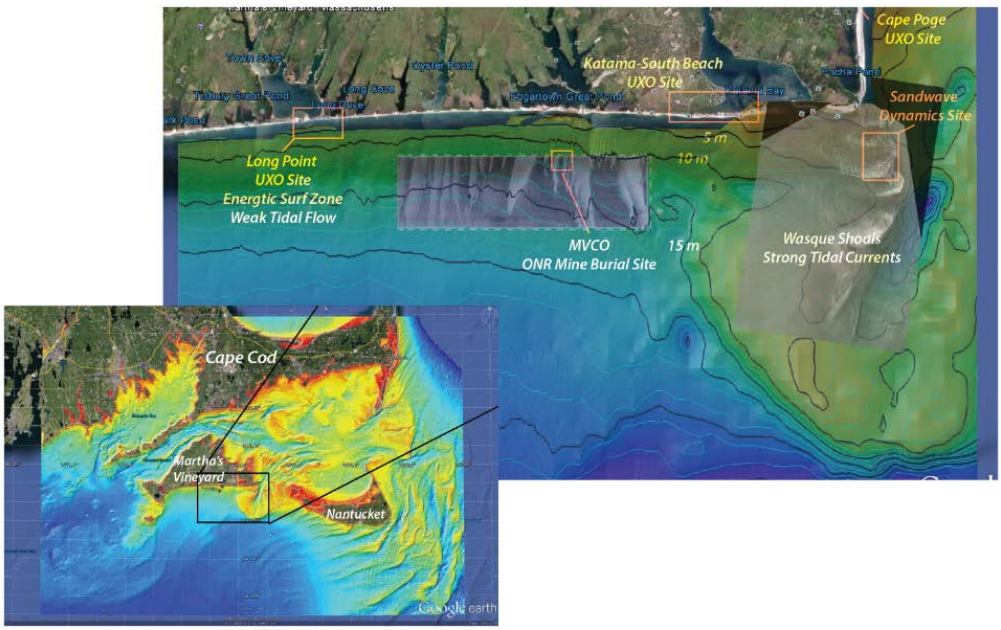

Figure 3. Location of study site and Cape Cod regional bathymetry, with aerial imagery of Wasque Shoals, and sidescan sonar imagery of the area near Martha's Vineyard Coastal Observatory (MVCO)

resulting in minimal migration. Measured migration distances were a maximum of 3 m. In the Duck study, the same density and size objects were deployed in a shallow field in 2.4 to 4 m water depth and a deep field between 6 and 7 m water depth. Wave heights were roughly similar to the Kauai study with small fair-weather waves and storms resulting in H_{sig}= 1.5 to 2 m at the shallow site. Maximum migration distances were 10 to 12 m, and the mean distance was 4.6 m. Maximum migration tended to occur at the beginnings of deployments when objects were not buried. At the end of the deployments, most objects either were buried by self-burial or sandbar migration. Similar to the Kauai deployments, due to the high density of the objects and relatively low wave energy (no 3 to 5 m wave height hurricane or large northeaster storm waves were experienced), migration distances were relative low. In both locations, the VORTEX MM produced migration and burial statistics consistent with the measurements. The measurements of object location were performed before and after energetic wave events, and no sensors were embedded in the UXO surrogates to record the exact time for the initiation of motion; thus, it was not possible to infer critical forcing conditions directly from the measurements. To measure the forcing conditions for the initiation of motion in the current study, motion sensors were embedded in the surrogate UXO. In addition, to extend the previous measurements to a high mobility regime, both size and density of the surrogate UXO were varied to ensure that some of the objects would migrate large distances in a single energetic wave event.

3. Materials and Methods

3.1. Location Study Sites

Two study sites were chosen off the coast of Martha's Vineyard, Massachusetts, to examine the differences between an environment with strong tidal currents and an energetic surf zone (Figure 3). In 2013 to 2014 (year 1), our work focused on Wasque Shoals, located near the southeast corner of Martha's Vineyard on ebb shoals of the Muskeget tidal channel between Nantucket and

Martha's Vineyard. Based on measurements in the ONR Sandwave Dynamics program, strong tidal velocities of 2 m/s are present in the channel but are reduced to 1 to 1.2 m/s at the surface on the ebb shoals study site location. Large tidal sand dunes with heights of 2 to 4 m in water depths of 4 to 8 m are present on the shoals and are visible in aerial imagery (Figure 3). The Wasque Shoals site is exposed to open ocean waves from the east-southeast to the west-southwest; however, the presence of shallow shoals (5 to 10 m depth) up to 10 km to the south of the study site will cause breaking of the largest waves and a reduction of wave energy at the study site compared to sites further west on the Martha's Vineyard south-facing coast. In year 2 (fall 2014), measurements were conducted at the Long Point Wildlife Refuge. Also referred to as the Tisbury Great Pond site, it served as a training range from 1943 to 1947 and has been the subject of remediation efforts (Figure 4; 17). Tidal currents are weak (0.3 m/s in the shore parallel direction) at this site compared to Wasque Shoals, but there is no shallow water offshore, so waves typically break within 1 km of the shoreline with little energy loss offshore due to breaking.

Figure 4. UXO (1) and notices to public at Long Point, MV

Based on 15 years of wave height statistics from the Martha's Vineyard Coastal Observatory (MVCO), waves are largest in the winter months (Nov.–March) except for rare hurricanes in the early fall (Figure 5). Thus, deployments typically took place in late September or early October to have slightly less energetic conditions for deployment, followed by energetic conditions during the deployment.

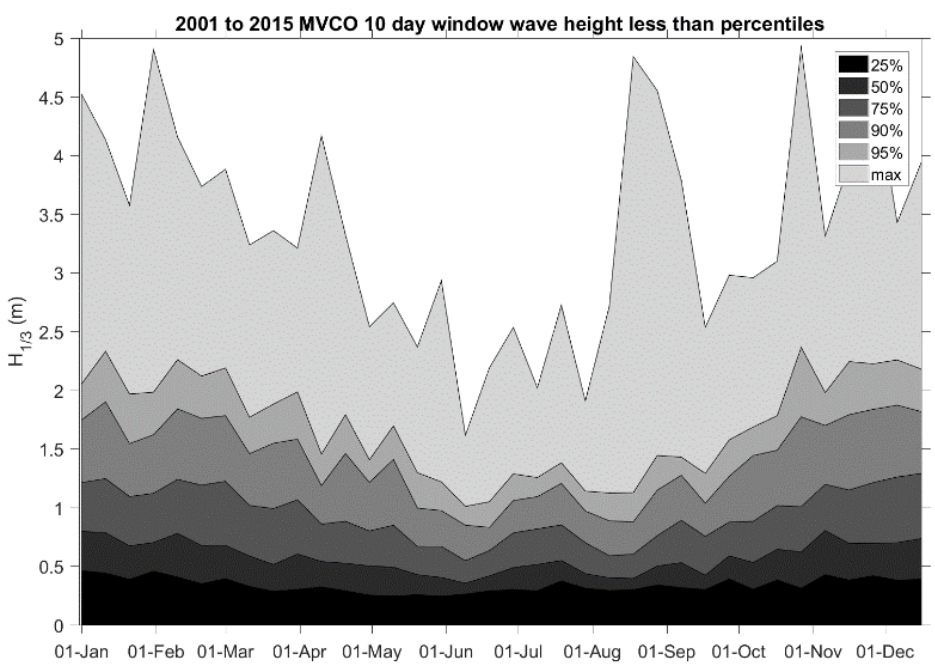

Figure 5. MVCO wave height statistics

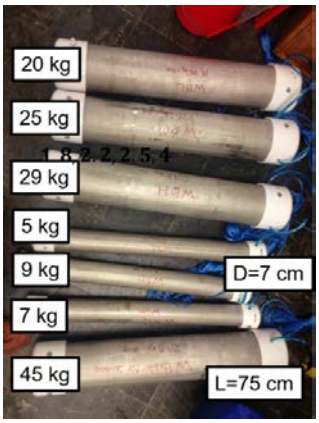

Figure 7. Surrogate UXO

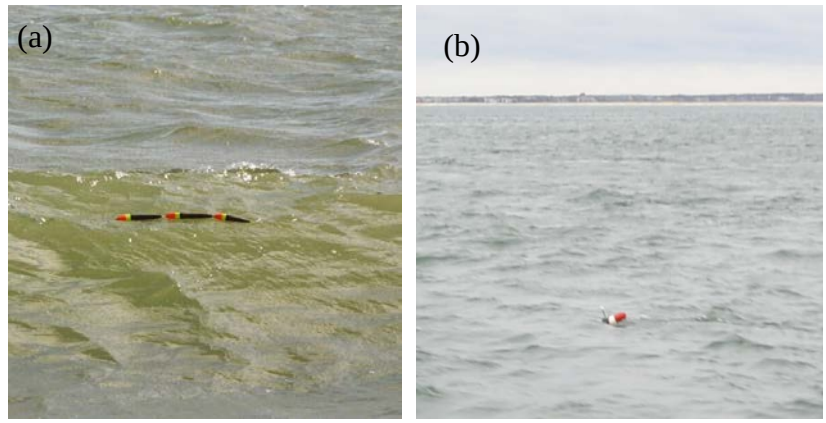

Figure 6. a) Passive tracking buoys and b) GPS tracking buoy

3.2. **UXO Surrogate Objects**

To measure UXO mobility and burial, a series of UXO surrogate objects were developed with internal motion sensors, acoustic tracking transponders, and both GPS and passive surface buoys. Due to the location of our field measurement sites at land trust and wildlife refuges, which had been used as former training ranges and are now undergoing remediation efforts (17), the surrogate UXO could not resemble actual UXO. For this reason, pointed nose sections and tail fins were not used, and a geometry of a straight cylinder was selected. The details of the exact specifications of each UXO surrogate are provided in Appendix A, but they were generally divided into two small diameters (D_0 = 7 cm) and large diameters (D_0 = 14 cm), and four different density classes (light: S_0 ~ 1.6 to 1.8, medium: S_0 ~ 2.1 to 2.2, heavy: 2.5 to 2.6, and very heavy: 3.8 to 3.9). The length of the objects for both diameters was fixed at 75 cm. The objects were fabricated from 0.25-inch wall-thickness grade 316 stainless pipe, with PVC endcaps and a mixture of concrete and lead ballasting to achieve the desired density (Figure 6). A Delrin and PVC pressure case contained the motion sensor and batteries.

3.2.1. GPS and Passive Buoys

To track the objects, a GPS tracking buoy was designed to have minimal drag, yet enough buoyancy to keep the GPS from becoming submerged except during the most energetic conditions (Figure 7). Because we could not find a suitable Commercial Off-The-Shelf (COTS) GPS logger with programmable sampling intervals to conserve battery power, and the correct geometry to be housed in a ¾ in ID tube at reasonable cost, we designed a logger from COTS components. The logger consisted of a Ublox Max-7Q module, a 3D Robotics 915 MHz RF serial radio for communications, and an MSP 430 microcontroller to schedule GPS acquisition and serial radio transmissions. The GPS sampled 5 minutes per hour, and the radio transmitted three times per day on an hourly interval to aid in relocating the buoys. To last for approximately 48 days, four 18650 series, 3.7 V, 2600 mAh nonrechargeable Li-ion batteries were required. Because the total weight of the batteries and electronics was 250 g, a substantial amount of buoyancy was required to keep the buoys afloat. Various buoy designs measuring 10 to 15 cm in diameter and 50 to 75 cm long were tested in a towing tank with speeds up to 2 m/s to optimize the trade-offs between drag and buoyancy to keep the GPS antenna exposed. In the 2 m/s steady flow velocity conditions of the flume, the drag on the buoys was 20 N with 2 times water depth scope on the buoy tether. Based on these results, we predicted that the buoy drag would not be substantial relative to the object mass for the large diameter objects (20 to 45 kg), but it could be

significant for the small diameter objects (5 to 7 kg). In actual field use at the Wasque Shoals wave and tidally forced environment, all the small diameter objects were transported out of the study area and not recovered, whereas the large diameter objects only migrated small distances. Based on this result from year one, we used a much smaller, low drag float (2 cm diameter, by 10 cm long) that would only produce 2 to 4 N drag at the Long Point surf zone experiment in year two. These floats could not support the GPS logger system, so they were used in purely passive mode with manual GPS tracking.

3.2.2. Embedded Motion Sensors

To measure the time of motion initiation of the surrogate UXO, an X-IO Inertial Motion Unit (IMU) logger was embedded in the large diameter objects (Figure 8). The X-IO IMU was set to record 3 axis accelerations, magnetic fields, and rotation rates for 10 minutes at 32 Hz to a micro SD card on waking up from sleep mode triggered by a high-acceleration event. The threshold for wake was set to the most sensitive setting so any subtle rolling motion of the UXO would begin data logging. The sensor has an onboard filtering algorithm to produce quaternion output format estimates of orientation (heading, roll, pitch) from the raw sensor data. After 10 minutes, the logger returns to a low-power state until another acceleration event occurs.

3.2.3. Acoustic Tracking Systems

To track the location of the UXO surrogates in real time, a USBL acoustic array developed for Remote Environmental Monitoring Underwater System (REMUS) autonomous underwater vehicles (AUVs) was adapted for deployment on a fixed frame or pole on the seafloor (Figure 9). The array consisted of 4 hydrophones in a square configuration separated by 25 mm across the diagonal. The system operated at 24 to 29 kHz. Each large diameter UXO surrogate was equipped with a transponder that would emit a coded signal in response to an interrogation signal from the USBL interrogation transponder. The interrogation pulses were set to occur on 15-minute intervals. The two-way travel time from the interrogation pulse and coded response is used to calculate a range to each object, and the 4-channel array produces an estimate of direction.

Testing at the WHOI dock with a fixed transponder and UBSL geometry during calm conditions indicated 1.2° root mean squared (r.m.s.) variations in heading and 0.3 m r.m.s. variations in range. The mean heading was within 0.7 degrees, and the range was within 5% (2 m difference over 50 m) of an estimate made on Google Maps using the USBL and transponder locations. Dock testing in very rough conditions (wind greater than 15 m/s) with large amounts of white-capping revealed fewer successful two-way travel time receptions and an increase in heading variations to 15° r.m.s. Field measurements of targets that were known not to have migrated

Figure 8. IMU mounted on the endcap of the pressure case inside a surrogate UXO

Figure 9. USBL array (left) and interrogation transponder (right)

from buoy location tracking indicated similar accuracies during calm conditions and a decrease in detected transmissions as waves and bubbles increased.

3.3. **Bathymetric Mapping Techniques**

One of the most important measurements for any study of UXO mobility is bathymetry. To measure bathymetry, we used the Jetyak (jet drive kayak hull) autonomous surface vessel recently developed at WHOI (Figure 10, 19). This hybrid remote control (RC) autonomous surface vessel (ASV) is capable of following GPS waypoint tracks with an accuracy of ±5 m, even in energetic tidal flow conditions, and can operate in 2 to 3 ft breaking waves in the surf zone (Figure 11). In larger waves, the RC can be used to pause a mission as a set of waves comes in and then resume. The 5.2 kW, 4-stroke gas engine provides top speeds of 5 to 7 m/s depending on sensor configuration and payload weight, with a typical survey speed of 2 m/s. The 11.4 L fuel tank allows for a run time of up to 8 hours before refueling. Bathymetry was measured using a combination of a 200 kHz downward-aimed echo sounder and a Post-Processed Kinetic (PPK) GPS system to resolve both horizontal and vertical positions within several centimeters (2–3 cm horizontal, 3–5 cm vertical). GPS positions were sampled at 10 Hz to accurately capture the vessel position while moving at 2 m/s and to capture the heave motions as the vehicle's vertical position is undulated by waves and tides. The GPS measurements were referenced to a Continuously Operating Reference Station (CORS) in Falmouth, Massachusetts (MAFA),

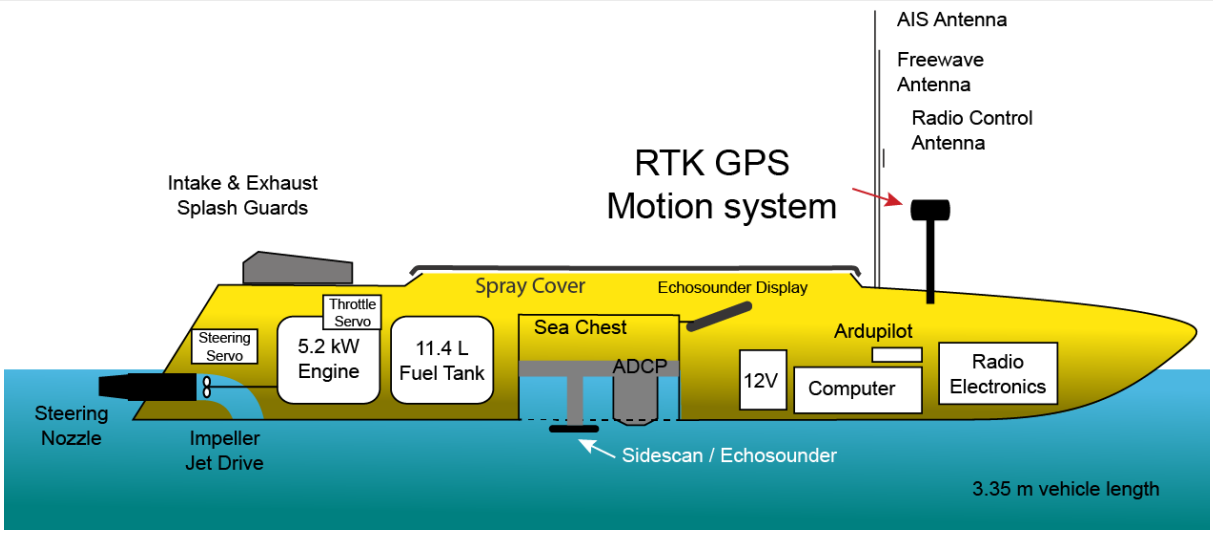

Figure 11. Schematic of Jetyak ASV System

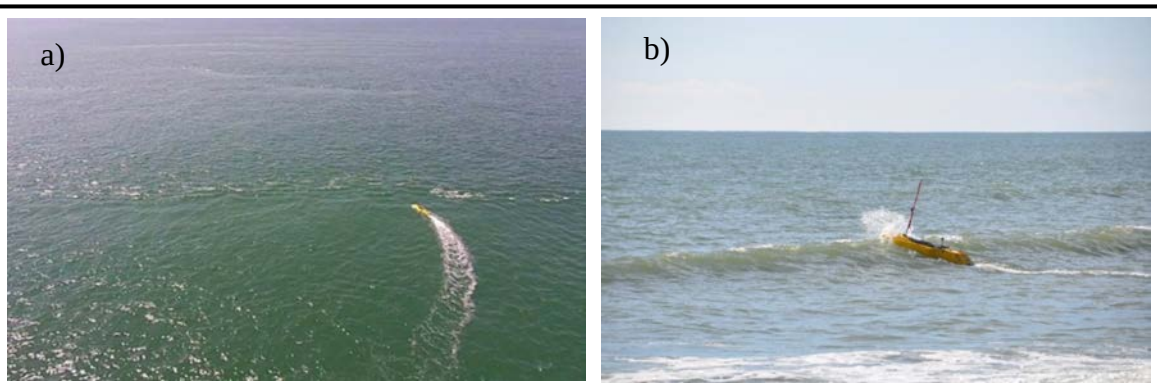

Figure 10. Jetyak surveying at (a) Wasque Shoals and (b) Long Point

allowing the bathymetry measurement relative to the well-defined NAD83 datum using the CONUS 12A geiod and NAVD88 vertical datum. In addition to bathymetry measurements at the Long Point surf zone site, beach topography was measured using a PPK GPS backpack system. A walking survey from the base of the foreshore dunes to 1 m water depth was performed at low tide and overlapped with the Jetyak bathymetry surveys performed at high tide.

The bathymetry, including small- and large-scale bedforms, has a leading order control on both the forcing hydrodynamics and object mobility and burial. In tidal flow environments, such as Wasque Shoals, the bathymetry of the shoals steers the flows and produces large asymmetries in the strength of ebb relative to flood tide at certain locations. Flows are also much stronger on crests of large-scale bedforms as the flows accelerate over the crests and decelerate in the troughs. In tidal shoal environments, waves can break both due to depth limitations and due to interactions with currents over the crest of large-scale bedforms (Figure 11a). The slopes associated with both large- and small-scale bedforms can trap UXO in the troughs and provide a significant barrier to large-scale mobility. Migration of the bedforms can bury objects to much deeper depths than scour burial alone. In surf zone environments, bathymetry controls the location of wave breaking and the structure of longer timescale currents generated by wave breaking. If there is an offshore sandbar with a trough between the beach and the bar, the trough is a likely location for the termination of UXO mobility.

3.3.1. Wasque Shoals Bathymetry

The large-scale bathymetry at Wasque Shoals is dominated by the ebb shoals of the Muskeget channel. The shoals to the west of the channel, where the measurements took place, have a series of large-scale tidal dunes that migrate toward the northeast in the direction of the flood-dominant

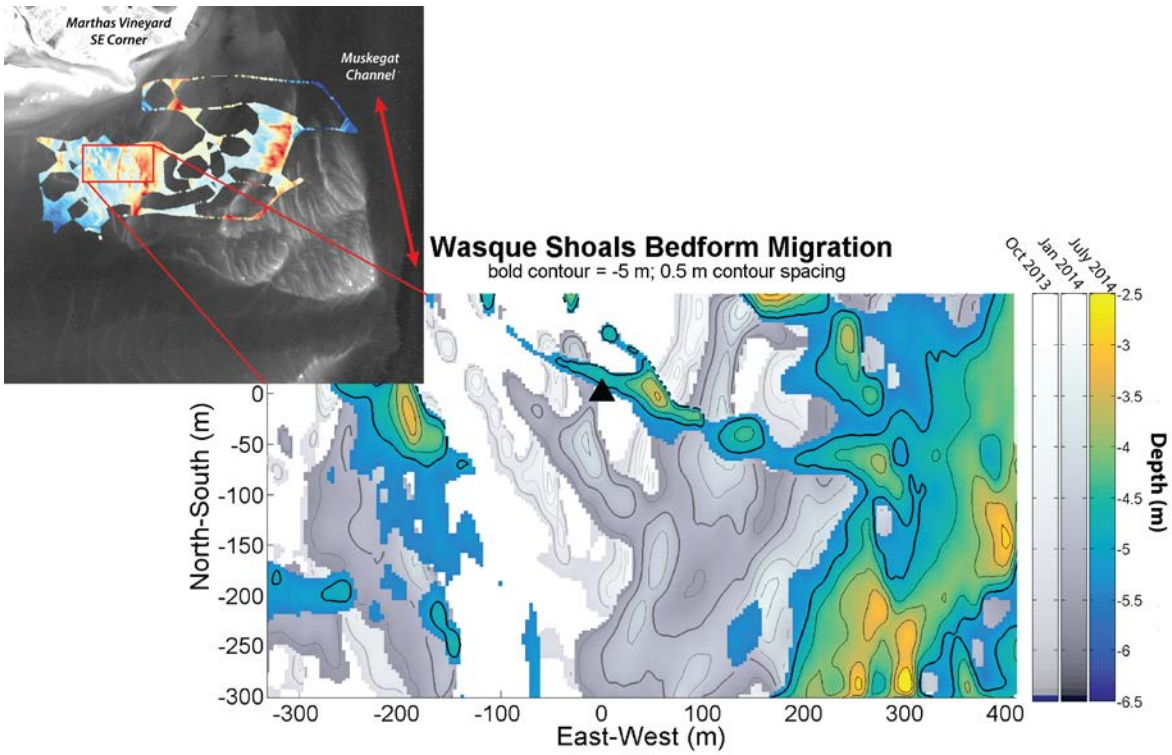

Figure 12. Bathymetry of Wasque Shoals in Oct. 2013, Jan. 2014, and July 2014, showing the migration of a large dune over our instrumented quadpod (location indicated by triangle)

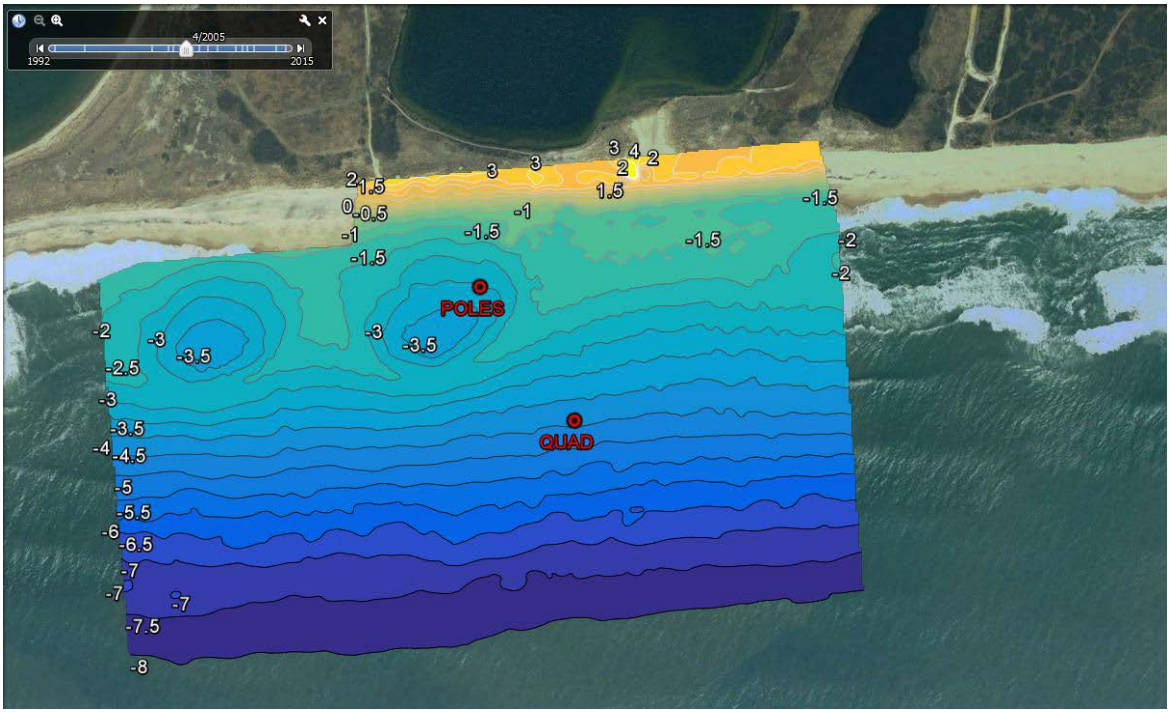

Figure 13. Long Point surf zone site bathymetry

tidal currents at this location. Surveys conducted in October 2013, January 2014, and July 2014 indicated 150 m migration of the approximately 200 m wavelength, 3 m high dune, partially burying and then eventually reexposing our 3.5 m high instrumented environmental monitoring frame (Figure 12). Portions of the shoals (southeast corner of imagery in Figure 12) become subaerial islands and then become subaqueous shoals in a 5- to 7-year period.

3.3.2. Long Point Surf Zone Bathymetry

The bathymetric and topographic surveys conducted at Long Point reveal a complex nearshore environment with an approximately 100 m wide and 1.5 m deep shelf or terrace in some locations and 3 m deep holes centered 100 m from the beach in other locations (Figure 13). The Google Earth imagery collected in 2005 during energetic wave conditions shows wave breaking on the shelf similar to the observed conditions during our deployment and offshore directed rip currents in the deep holes. In the imagery, wave breaking on the shelf ends approximately 30 m from the shoreline, also consistent with observed conditions during our deployment. On the terrace, there is a slight trough, deeper than 1.5 m but not reaching 2 m, located 20 m from the shoreline (0 m contour). Environmental monitoring sensors were deployed on a four-legged frame (quadpod) in 4.5 m water depth due to the constraints of deployment from a ship large enough to handle the frame. A second set of sensors was deployed on poles jetted into the seafloor in the eastern hole because wave breaking was less intense in the hole and allowed easier small boat operations (Figure 14).

3.4. **Measurement Techniques for Forcing Hydrodynamics and Small-Scale Bedforms**

At both the Long Point surf zone site and the Wasque Shoals tidal site, large (2.5 to 3.5 m high) seafloor-mounted quadpods were deployed to measure hydrodynamic forcing and small-scale bedforms. At Wasque Shoals, the frame had two Nortek Vector Acoustic Doppler Velocimeters (ADVs) with pressure sensors to measure nearbed flow, waves, and turbulence; a WHOI Pulse-

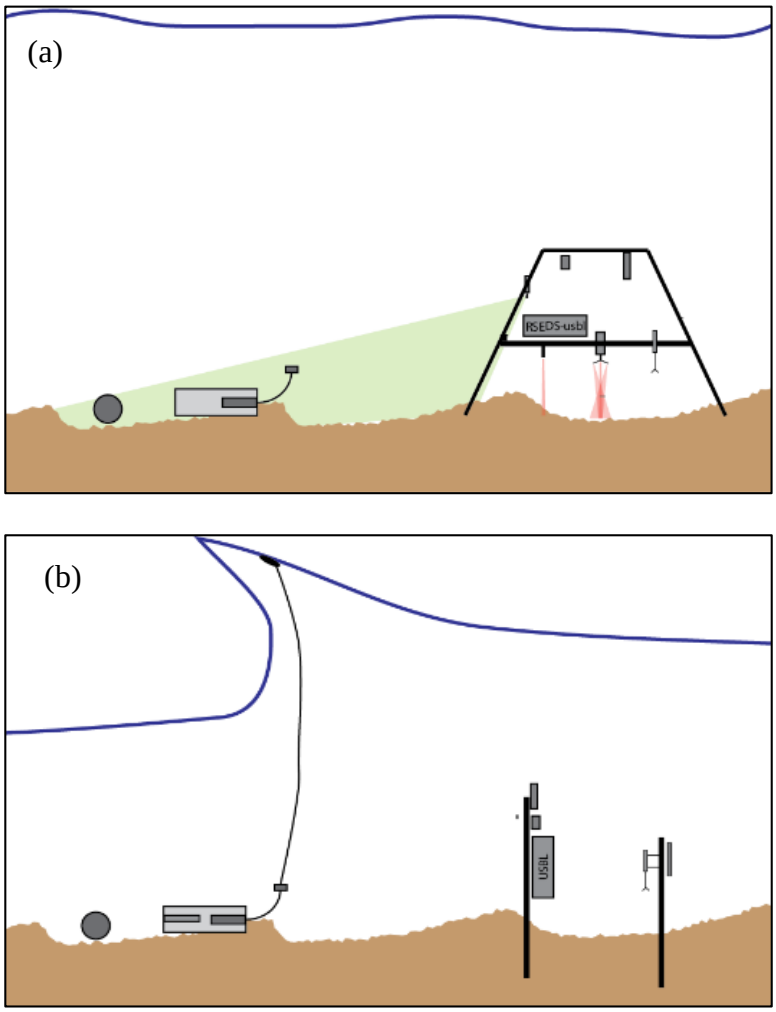

Figure 14. Schematic of (a) a quadpod and (b) pole mount sensors

Coherent Doppler Profiler (PCDP) to measure nearbed flow and backscatter; an Aquatec Acoustic Backscatter Sensor (ABS) profiler to measure profiles of backscatter; a Nortek Aquadopp to measure the profile of the nearbed tidal flow; a Nortek Acoustic Wave And Current (AWAC) profiler to measure column flows and waves; an Imagenex 881A rotary fan-beam sidescan to measure small- to medium-scale bedforms; and an Imagenex Delta-T multibeam mounted in a rotary side-looking configuration to measure medium-scale bedforms (Figure 15).

The quadpod deployed at Long Point (Figure 16) had a similar set of instruments, except it did not have the AWAC or the Aquadopp, and the side-looking multibeam was swapped for a 2-axis rotary pencil-beam sonar. Nearbed hydrodynamic sensors were set on sampling schedules to resolve waves, turbulence, and longer timescale processes such as tides while conserving battery power (e.g., a 10 Hz burst of 15 minutes once per hour). Bedform imaging sonars were too power consumptive and slow sampling to resolve individual waves, so they were set to sample longer timescale processes. For instance, rotary sonars used a burst of 6 images once every 20 minutes, which could be averaged to reduce noise. Rotary sidescan sonars also typically used a long (10 m radius) and short (5 m radius) range setting for resolving both medium- and small-scale features as the number of range samples on this sonar is fixed at 1,000.

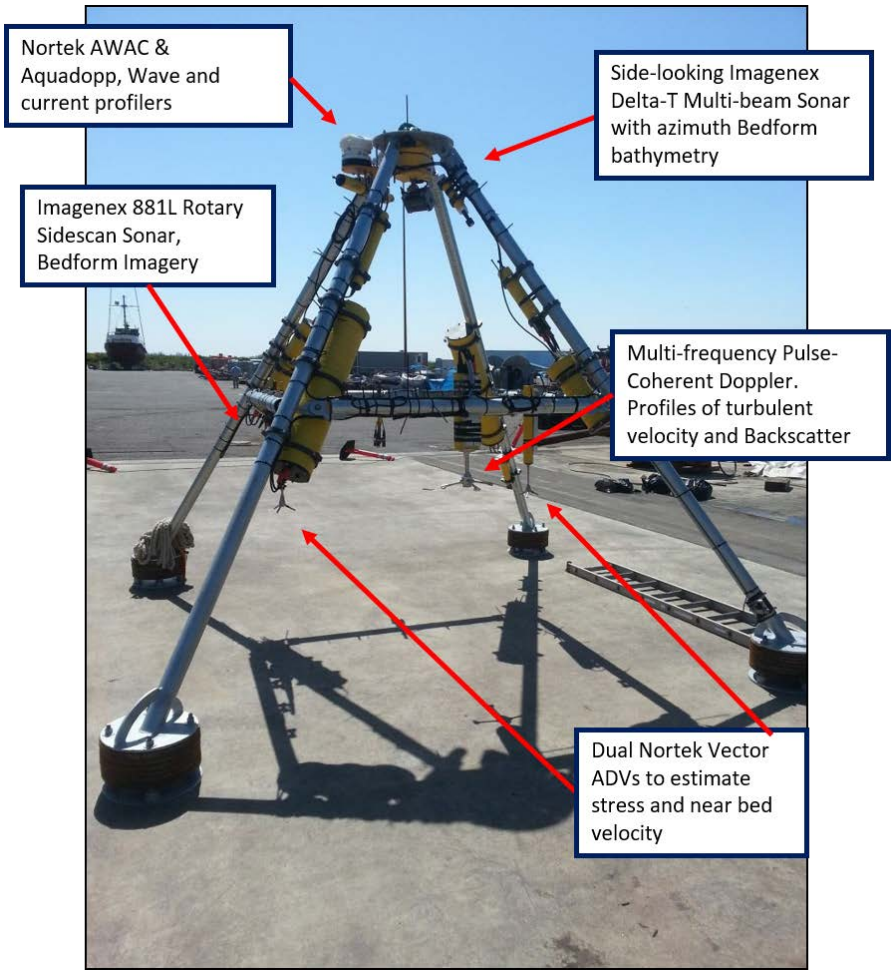

Figure 16. Quadpod and instruments at Wasque Shoals

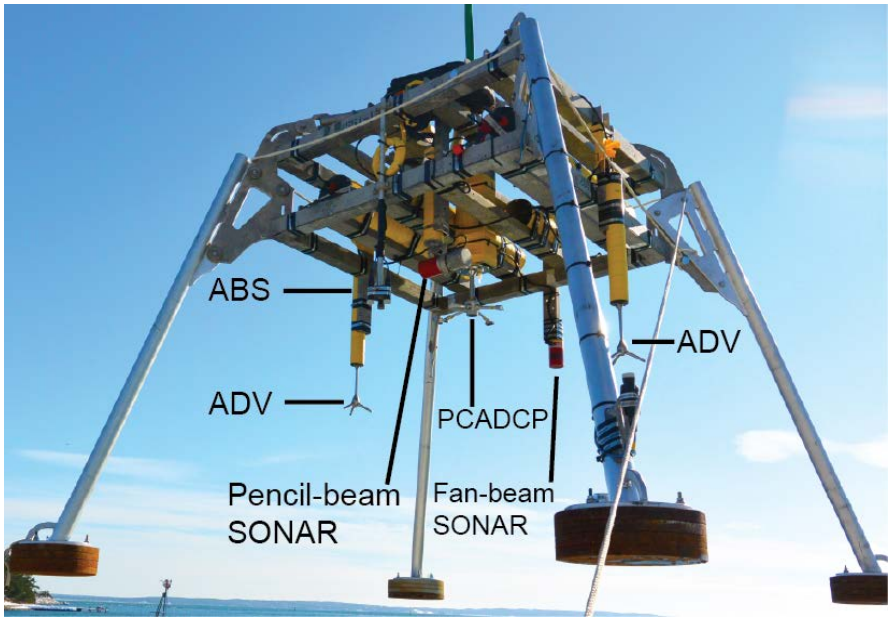

Figure 15. Quadpod and instruments at Long Point

4. Results and Discussion

4.1. **Wasque Shoals**

4.1.1. Hydrodynamic forcing

The instrumented quadpod measured tidal flow and waves from deployment on November 20, 2013, until the end of January, 2014, when the frame was partially buried by a 3 m high migrating dune. The exact date of burial of individual instruments depended on their mounting height, as lower instruments were buried earlier. Instruments were not recovered until May through September, 2014, when the frame gradually became unburied as the dune migrated past. The ABS provides a record of bed elevation increase as the dune migrates under the frame (Figure 17). The pressure sensor shows 1.2 m tidal depth variations during spring tides (day 3, 17, and 33) and 0.5 m variations during neap tides (day –4, 10, 24). Depth variations of ~0.2 m with timescales of ~2 to 3 days are also present during storms. Tidal velocities during spring tides are 1 m/s during flood tide and 0.75 m/s during ebb. During neap tides they are reduced to 0.5 m/s. Measured tidal velocities increase slightly through the deployment as the water depth becomes shallower due to dune migration and as the flows accelerate over the dune crest.

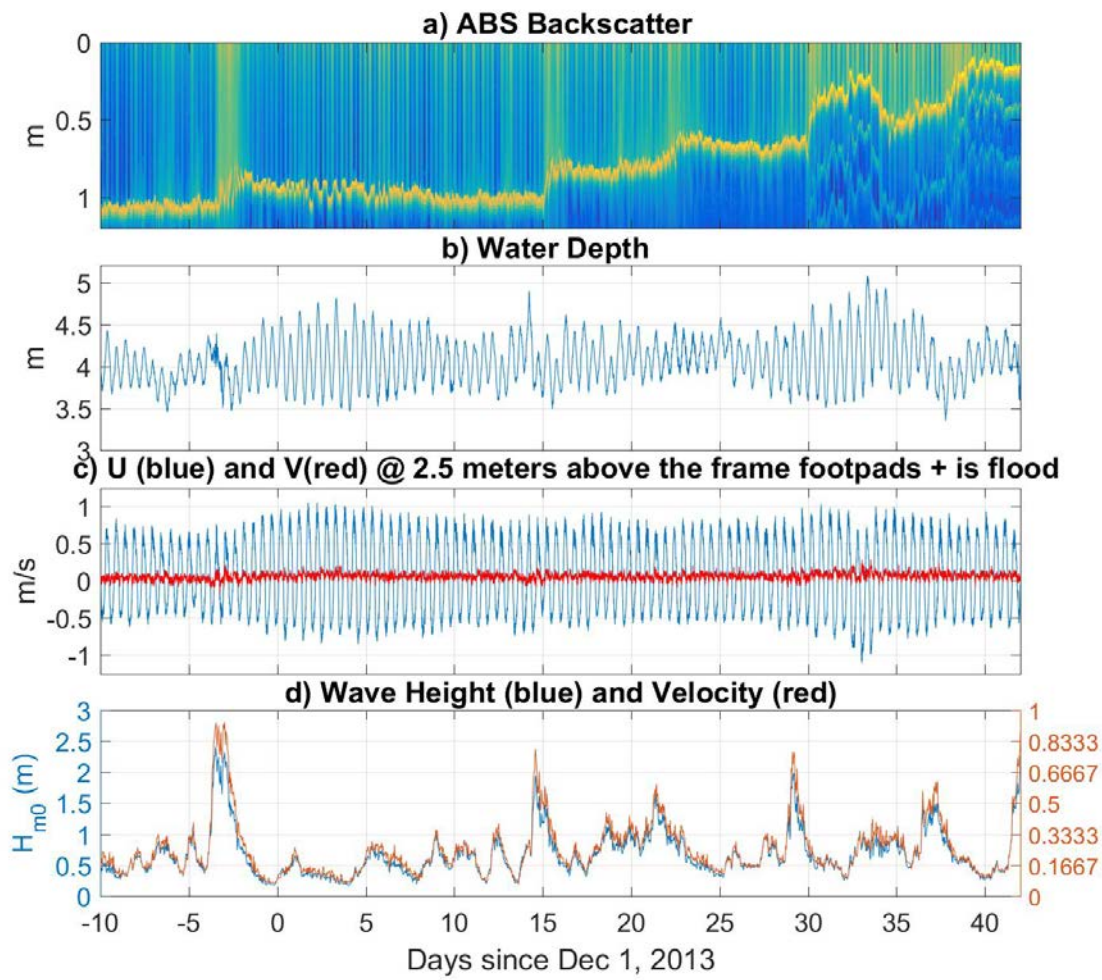

Figure 17. Time series of downward-aimed acoustic backscatter and hydrodynamic sensors from Wasque Shoals

Wave heights are typically 0.5 to 1.0 m in fair-weather background conditions and increase to 2 to 3 m during storms (day -2, 15, 22, and 29). Nearbed representative orbital velocities follow a similar trend to the wave heights with background levels of 0.1 to 0.25 m/s and increasing to 0.7 to 0.8 m/s during energetic wave conditions. The spectral distribution of wave energy is quite wide with a typical swell peak at 0.1 Hz and sea energy up to 0.3 Hz (Figure 18). Toward the end of storms, the high frequencies seas subside, and only the swell remains. Higher frequency turbulent velocity fluctuations ($f > .4$ Hz) are tidally modulated and generated by strong tidal current flowing over the large dunes and mega-ripples. Wave skewness and asymmetry have been shown to be important (11, 20, 21) in forcing ripple migration and other sediment transport processes, thus they have potential to be important for UXO migration. The unnormalized forms of skewness $\langle U_w^3 \rangle$ and asymmetry $\langle H(U_w^3) \rangle$, where $H(U_w^3)$ is the imaginary part of the Hilbert transform of U_w^3, are shown in Figure 18 because normalized skewness ($Sk = \langle U_w^3 \rangle / U_{w,rms}^3$) and asymmetry ($As = \langle H(U_w^3) \rangle / U_{w,rms}^3$) are not reliable estimates due to low Signal-to-Noise Ratio (SNR) during periods of low wave velocities. Here U_w are the instantaneous wave velocities in a burst, as opposed to the burst average representative wave velocity (U_{wbr}). $\langle U_w^3 \rangle$ is relatively high during storms with values of around 0.1, corresponding to $Sk = 0.4$, while asymmetry is relatively low with values of $\langle H(U)_w^3 \rangle$ around 0.015, corresponding to $As = 0.1$. The asymmetry appears to vary on a tidal timescale, thus it could be modulated by wave current interaction due to the strong flow and wave energy convergences on the large dunes. The skewness is always positive in the direction of wave propagation.

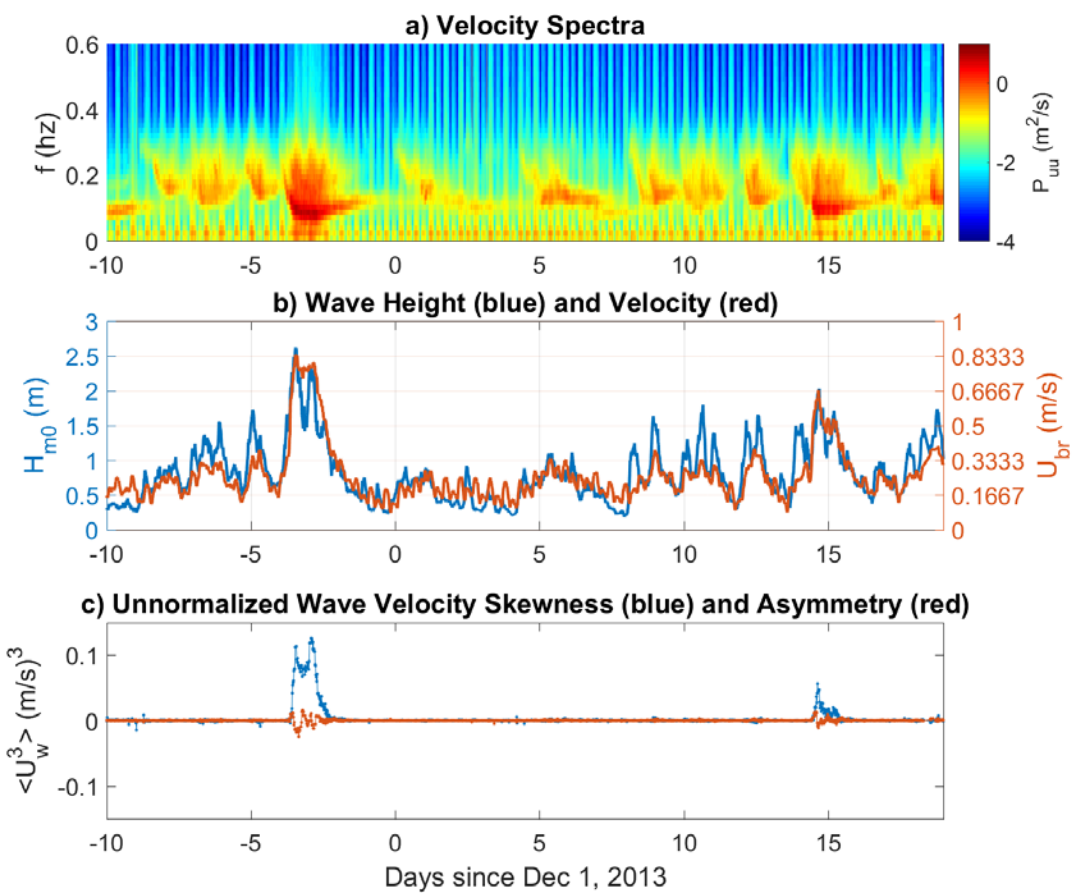

Figure 18 Time series of wave parameters on Wasque Shoals

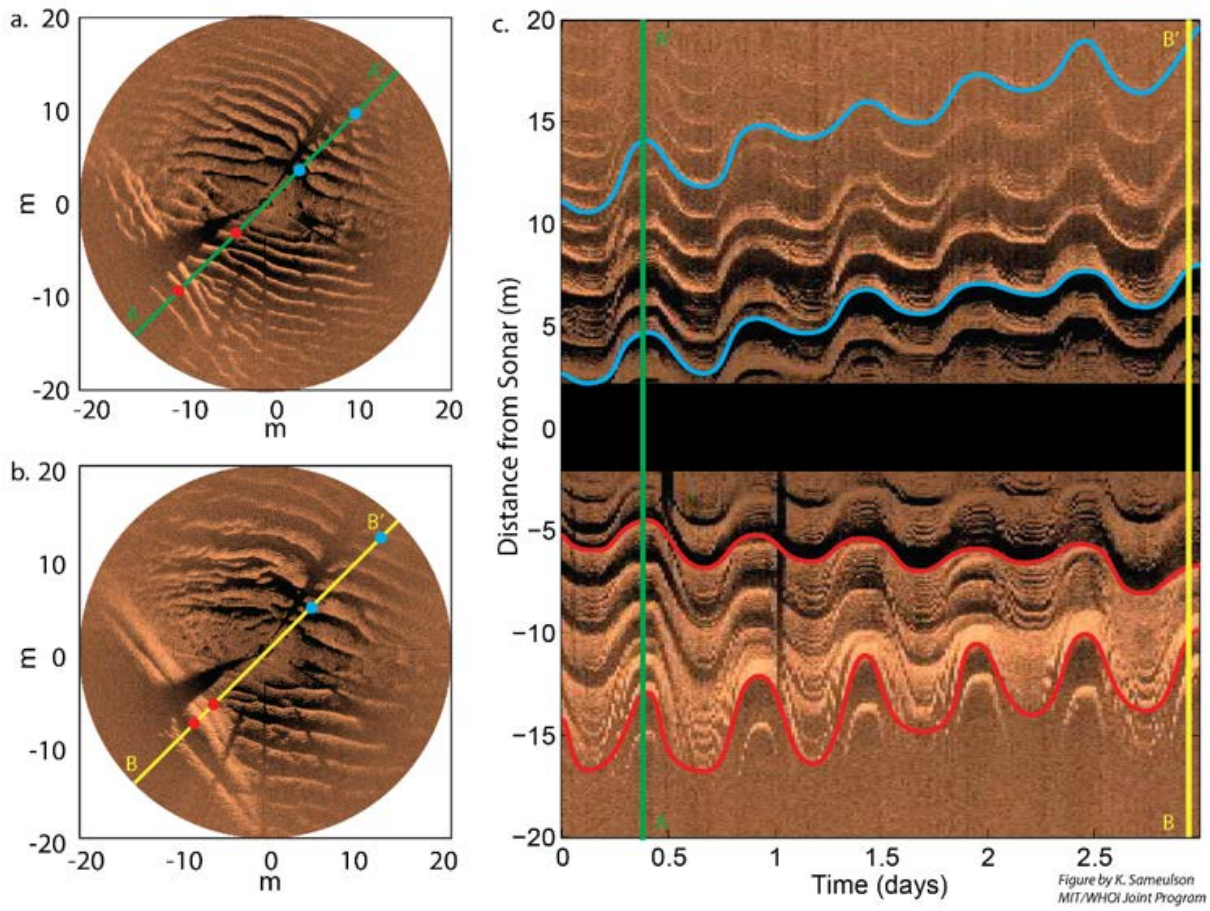

Figure 19. Rotary sonar imagery showing migrating mega-ripples and the beginning (a) green transect in (c) and end (b) yellow transect in (c) of a three-day period. Sidescan backscattered intensity along the transect shown by the green and yellow lines reveals the convergence and divergence of the migrating mega-ripples.

4.1.2. Small-Scale Bedforms

Rotary sidescan sonar imagery with long-range sensor settings reveal small-scale bedforms known as tidally reversing mega-ripples (22). These features have 1 to 5 m wavelength and 10 to 50 cm height, and thus are larger than typical current-formed ripples that scale with a grain diameter ($\lambda \sim 1000 D_{50}$ = 30 cm), but they are much smaller than the large-scale dunes with ~100 m wavelength (Figure 19). The mega-ripples migrate approximately one wavelength on each half-tidal cycle and change asymmetry in the direction of migration with a significant lag relative to hydrodynamic forcing. Work in progress by MIT-WHOI PhD student Katie Samuelson is examining the role of sediment transport associated with small-scale bedform migration on large-scale dune dynamics (23). Initial analyses show that mega-ripple migration diverges in the trough and stoss face of large-scale migrating dunes and converges on the advancing lee face. Previous work on this subject indicates that while multiple scales of bedform may exist simultaneously, they do not dynamically interact. Samuelson's analysis of the new observations, with greater resolution and duration than previous measurements, suggests the opposite, that is, that the convergence and divergence of mega-ripple migration directly forces large-scale dune migration and morphology.

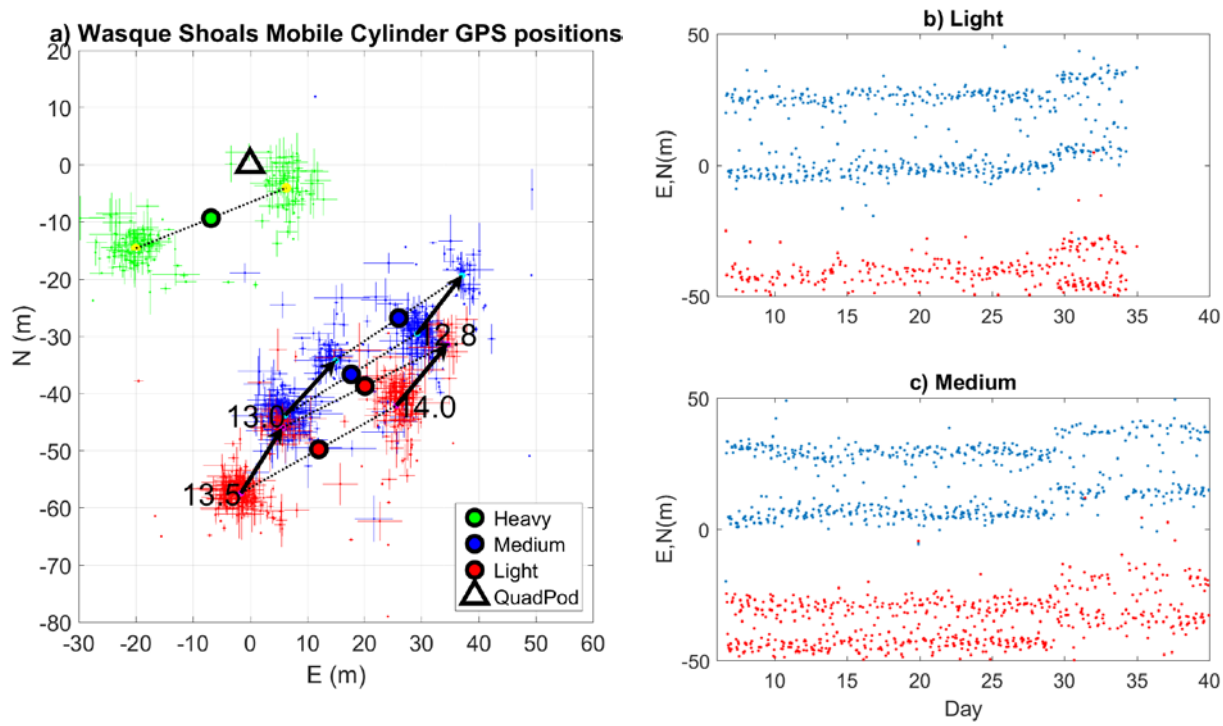

Figure 20. (a) Location of GPS buoy-tracked UXO at Wasque Shoals relative to quadpod and time series of (b) light and (c) medium density GPS buoy-tracked UXO locations

4.1.3. UXO Surrogate Deployments

4.1.3.1. Surrogate Mobility

At Wasque Shoals, 7 targets (4 large diameter and 3 small diameter) were deployed. As mentioned previously, all small-diameter targets were lost from the study area due to excessive drag from the GPS tracking buoys and were not recovered. The locations of the Heavy (WBH), Medium (WBM), and Light (WBL) buoys relative to the quadpod are shown in Figure 20. The location was calculated by the center of the two GPS point clouds as the GPS buoy shifted location due to the scope of the tether lines in the tidal currents. Based on the GPS buoy point clouds data, the heavy surrogate was not mobile. During recovery operations, it was found to be buried deep below the seafloor due to large-scale dune migration, and it was not recovered. Both the light and the medium surrogates were mobile and migrated approximately 13 m to the northeast during the storm on day 29 (Figure 20). At the time of recovery operations, these were not buried. While the GPS buoys provide data on the total distance of migration, the data do not constrain the exact timing of the initiation of motion due to the variations in buoy position associated with the scope of the tether line. The IMU data provides a time for the initiation of motion that can be used to look up the relevant forcing hydrodynamic parameters measured at the quadpod at this time (Figure 21). Because the surrogates were located tens of seconds of meters from the instrumented frame, and the clocks had differential drift errors of tens of seconds, the forcing conditions were examined on a burst-averaged timescale. The burst-averaged representative wave velocities were used as opposed to instantaneous wave orbital velocities.

The IMU data indicates that the light and medium objects were mobile on the high wave events of day 14 and 29 (Figure 21). During the periods with large surrogate orientation variations, the

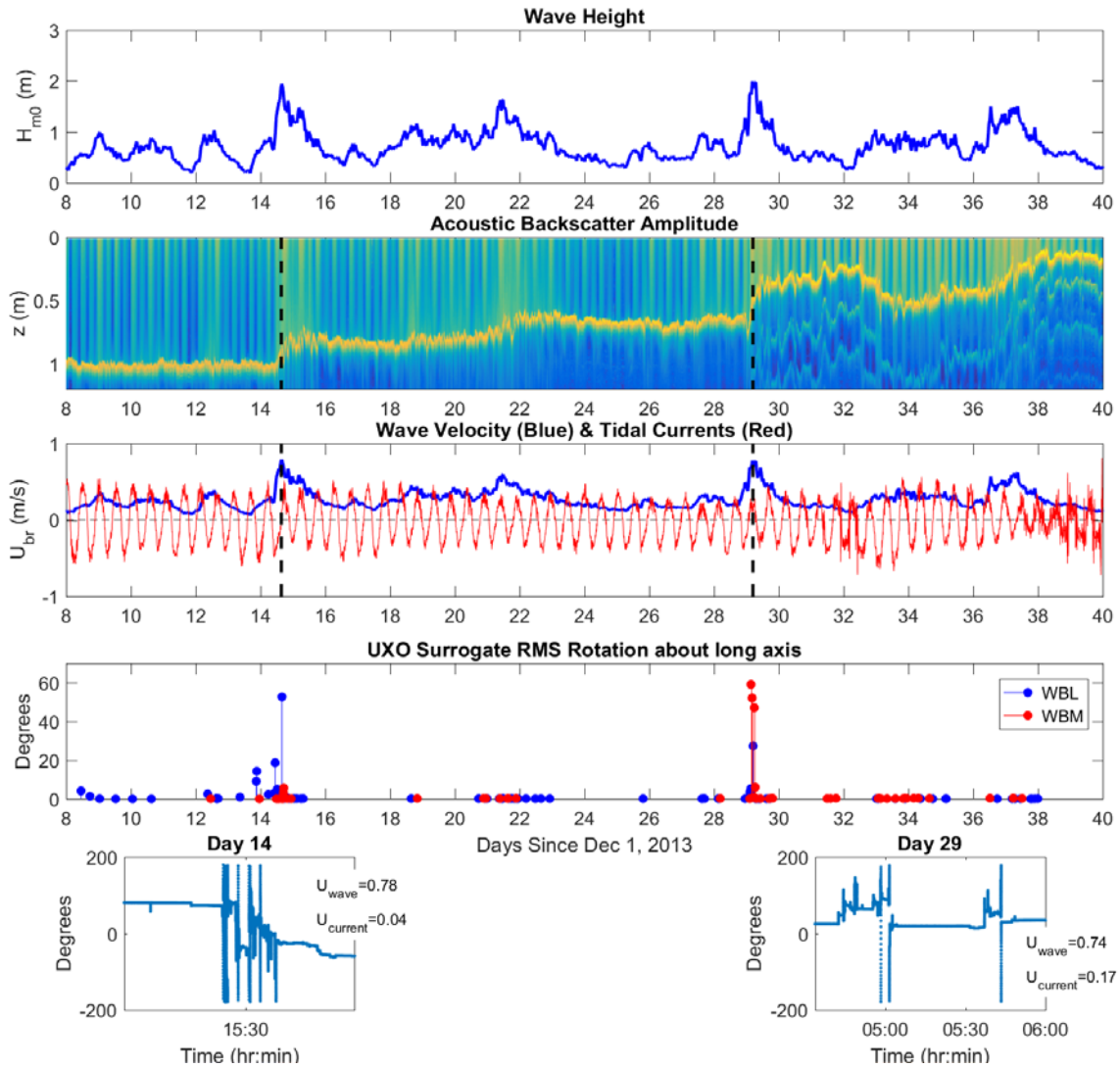

Figure 21. Time series of hydrodynamic and migrating bedform forcing and UXO mobility based on IMU data from Wasque Shoals

nearbed (z = 0.40 m) tidal currents were weak (~0.04 to 0.17 m/s), and wave velocities were strong at 0.7 to 0.8 m/s. Both events had similar wave orbital forcing, yet the second event resulted in a 13 m migration, while the first resulted in little to no migration.

The bathymetric surveys performed on October 16, 2013 (day –46), 36 days before deployment of the surrogates, and on January 10, (day 40), 11 days after the migration event, show the location of the dune relative to the targets on these two days. Although there was no survey near the storm on day 14, which caused mobility but no migration, based on the surveys on day 46 and day 40, the surrogates were most likely in the trough of the dune at this time. The ABS data shows 15 cm of elevation change during the storm and little elevation change on the spring tides on day 17, suggesting that both the quadpod and the surrogates were in the trough of the dune. On day 40, the survey reveals that the steep dune lee face is close to the original location of the surrogates before migration. The ABS elevation data indicate the seafloor rises on day 29, consistent with dune migration to the east, and then falls on a storm with waves from the northeast, suggesting the dune reversed and migrated to the west. The period of rapid migration

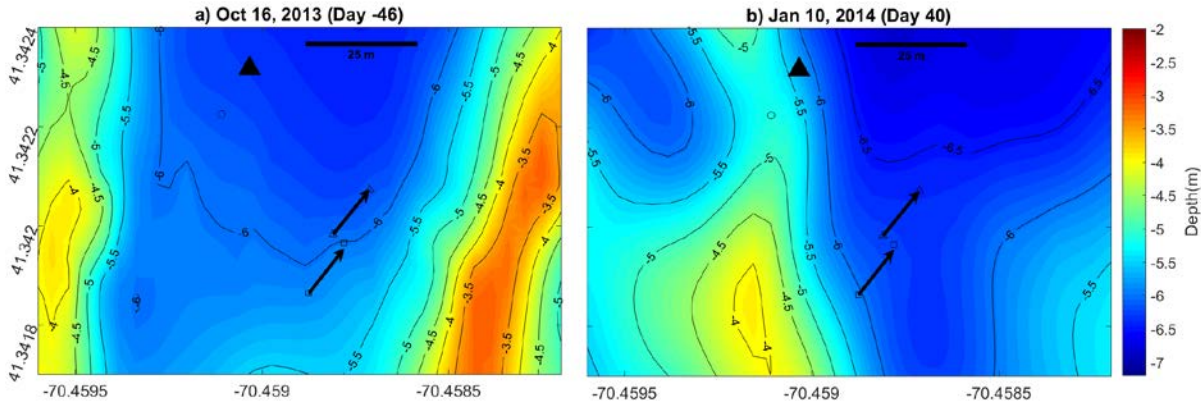

Figure 22. Migration paths of light and medium surrogate UXO superimposed on bathymetry (a) before the beginning of the depoyment and (b) at the recovery

to the east on day 29 most likely increased the bathymetric gradients near the objects, and the objects migrated from a region of steep slopes of 13 m to a region of lower gradients, essentially rolling into the trough of the large dune (Figure 22). On the storm of day 14, the objects were mobile, indicating the threshold for initiation of motion had been exceeded; however, the object did not migrate due to the lack of a large bathymetric gradient or due to trapping by the medium-scale mega-ripples. On day 29, the combination of conditions exceeding the threshold for motion and a steep bathymetric gradient (~0.1 to 0.2) allowed migration. However, in this environment of large dunes, the migration is constrained to be less than a quarter of the wavelength of the dunes, as the steep lee face only has an extent of approximately 15m.

In addition to the bathymetric control of object mobility, mobility also appears to be strongly linked to wave orbital velocity, even though there are strong tidal currents (greater than 1 m/s) at this location. Figure 23 shows that most points with high orientation variance occur at wave velocities greater than 0.6 m/s; however, there are some points with low, but nonzero, orientation variance at current velocities over 0.3 m/s.

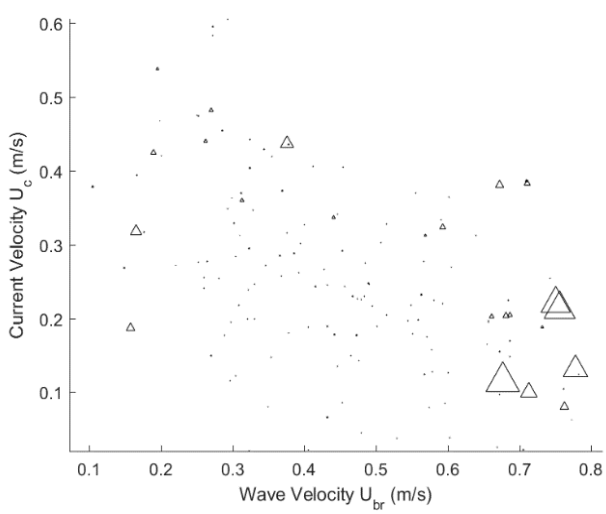

Figure 23. Scatter plot of UXO roll r.m.s. variations (indicated by size of symbol) vs. current and wave velocity

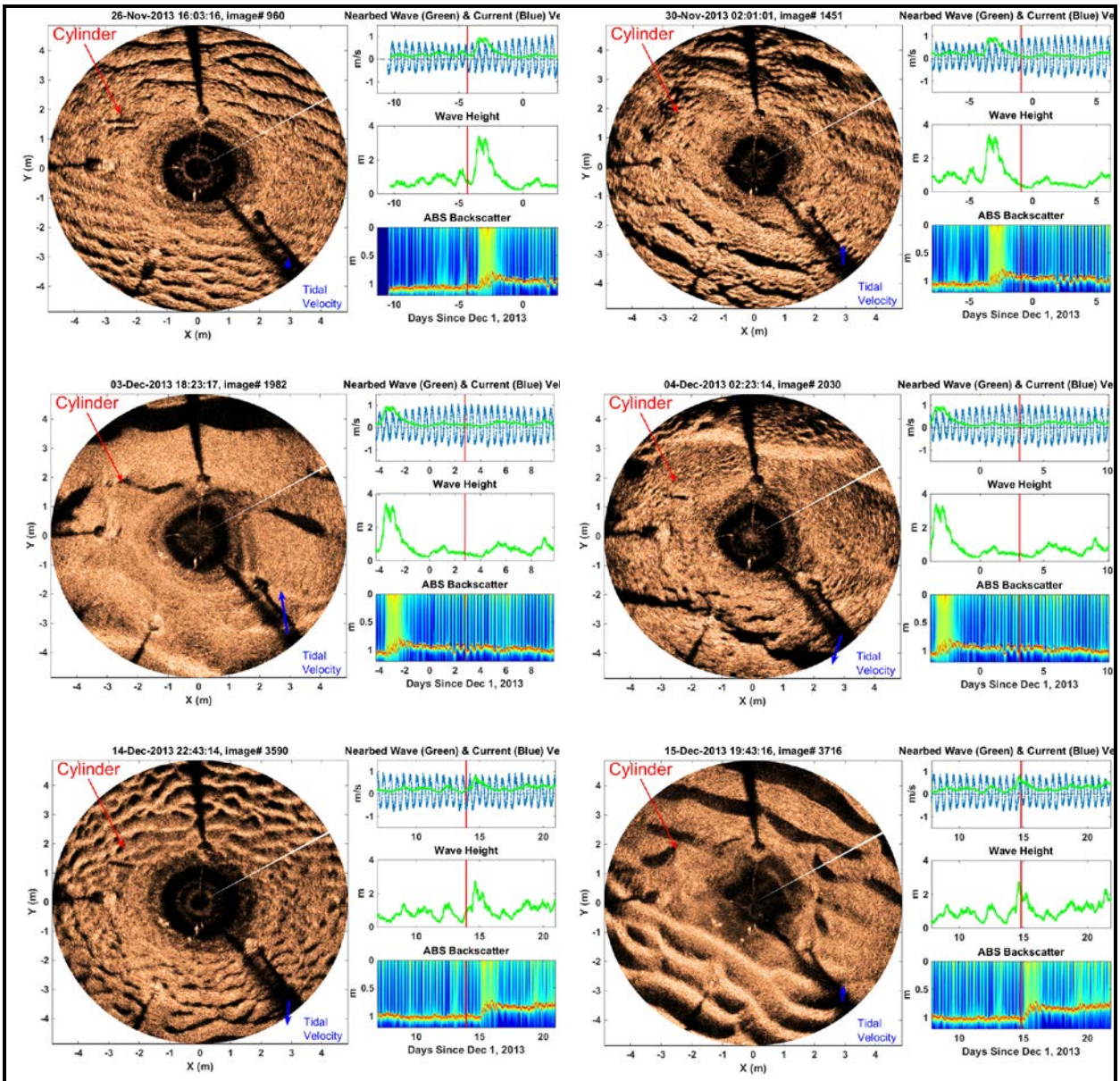

Figure 24. Succesive rotary sonar images showing transient burial and reexposure of a surrogate UXO by migrating mega-ripples at Wasque Shoals

4.1.3.2. Surrogate Burial

While the light and medium objects were mobile and not buried during this deployment, both the heavy (deployed 15 m from the quadpod) object and very heavy object (deployed 3 m from the quadpod) were buried and not recovered. The depth of burial was unknown as the tether leading to the heavy object snapped during recovery operations. The very heavy object was in the view of the rotary sonar, which documented a period of transitional burial by migrating mega-ripples, before deep burial by the migrating dune (Figure 24). Before the wave event on day –5 (Nov. 26, 16 hrs), the object was always visible. After the bed elevation increase on day –2.5, the object was buried for several days (Nov. 30, 02 hrs) but became visible in the troughs of the migrating mega-ripples on day 2 through day 6 (Dec. 3–4). The object was last visible in the sonar imagery on day 14 (Dec. 14), and after the bed elevation increase on day 15, it was buried for the remainder of the deployment (Dec. 15 onward).

4.2. **Long Point Surf Zone**

The Long Point surf zone UXO mobility experiments took place in the fall of 2014. An instrumented quadpod was deployed on September 16, 2014, in 4.5 m depth water, approximately 150 m offshore of the beach (Figure 13 and Figure 16). Six large-diameter surrogates with USBL tracking transponders were deployed at this time in depths ranging from 3 to 4 m. These objects have the first letter D for the deeper deployment depth, and then either L for light, M for medium, H for heavy, or UH for ultra-heavy to indicate the relative density (Appendix A). The frame was held in place with 2 m long poles jetted into the seafloor. Unfortunately, during the second major wave event of the deployment on September 22, the brackets connecting the poles to the frame failed, and the frame broke loose and migrated across the surf zone and onto the beach over the next three days. A second set of instruments with an additional USBL tracker and ADV was deployed on single poles jetted into the seafloor on September 19. These instruments were deployed in 3 m depth water, approximately 75 m from the shoreline on the northeast corner of a bathymetric depression in the nearshore topography. This location was chosen because the depth in the depression caused medium height waves to break less frequently there than the adjacent shallow shelf, which facilitated deploying and

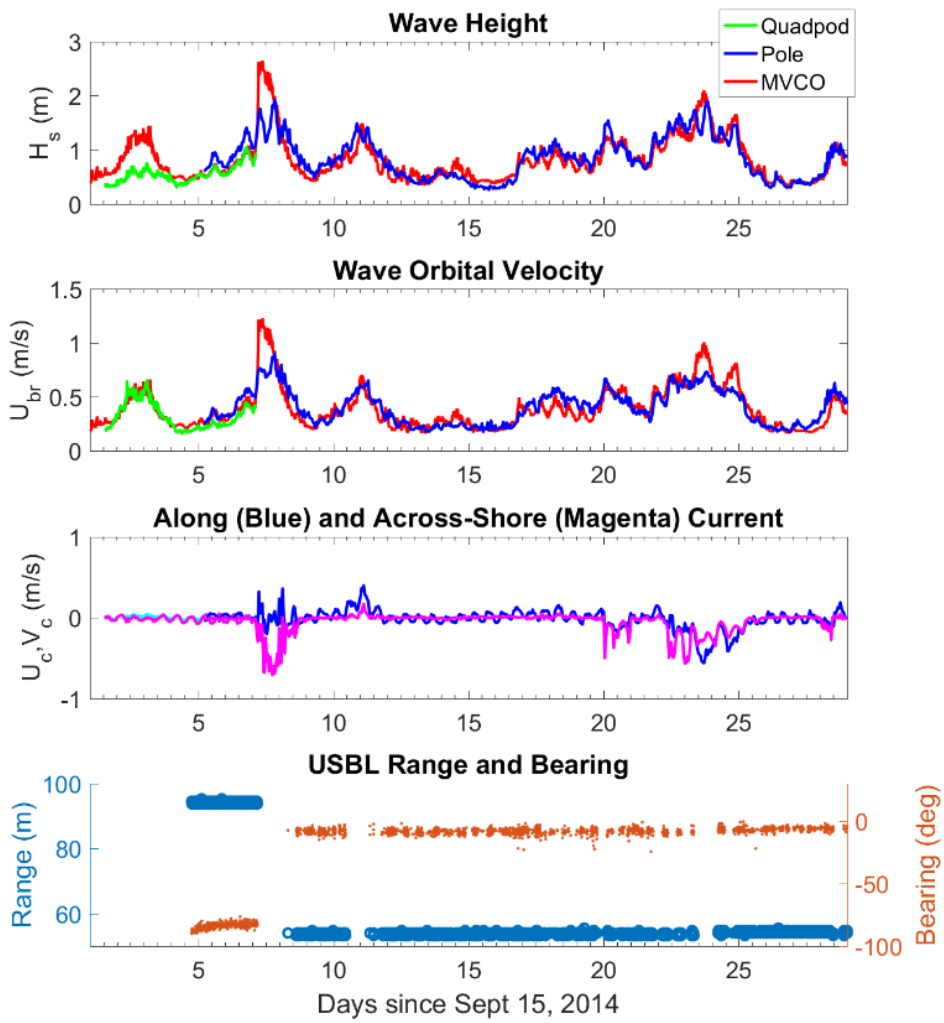

Figure 25. Time series of hydrodynamic forcing (upper panels) and USBL range and bearing (lower panel)

servicing the instruments. A second set of large-diameter surrogates were also deployed in water depths from 1.7 to 3.4 m at this time. The labels of these surrogates start with an uppercase S, indicating the shallower deployment depths. A set of small diameter surrogates, designated by the lowercase s, was deployed on October 4. Based on the experiences with high drag with the GPS buoys at Wasque Shoals, only small-diameter (5 cm or less), low buoyancy, passive floats were used at Long Point in addition to USBL transponders for tracking.

4.2.1. Hydrodynamic Forcing

a) Hydrodynamic forcing parameters were measured from both the quadpod Nortek Vector ADVs and the pole-mounted Vector ADV, and they were calculated from MVCO 12 m depth node b) ADCP data using linear wave theory to account for the depth difference between the quadpod and the 12 m node for orbital velocity calculations (Figure 25). Similar to the data at Wasque Shoals, storms during the Long Point measurements had wave heights of 1 to 2.5 m, and background wave heights were typically 0.5 m. The wave heights of the largest storms (H_s > 2 m) show a considerable reduction of wave height at the pole mount or quadpod sensor relative to MVCO, presumably due to wave breaking offshore of the nearshore sensors. Representative orbital velocities (U_{br}) were also similar to the Wasque Shoals deployment, with maximum values of ~0.9 m/s at the pole-mounted sensor and typical values of 0.5 to 0.7 m/s during storms. Unlike Wasque Shoals, tidal currents are weak at the Long Point surf zone site (U_{tidal} < 0.1 m/s), while wave-driven mean flows are much stronger with values up to 0.7 m/s. The wave-driven mean flows at the pole-mounted sensor were often dominated by cross-shore currents as a strong

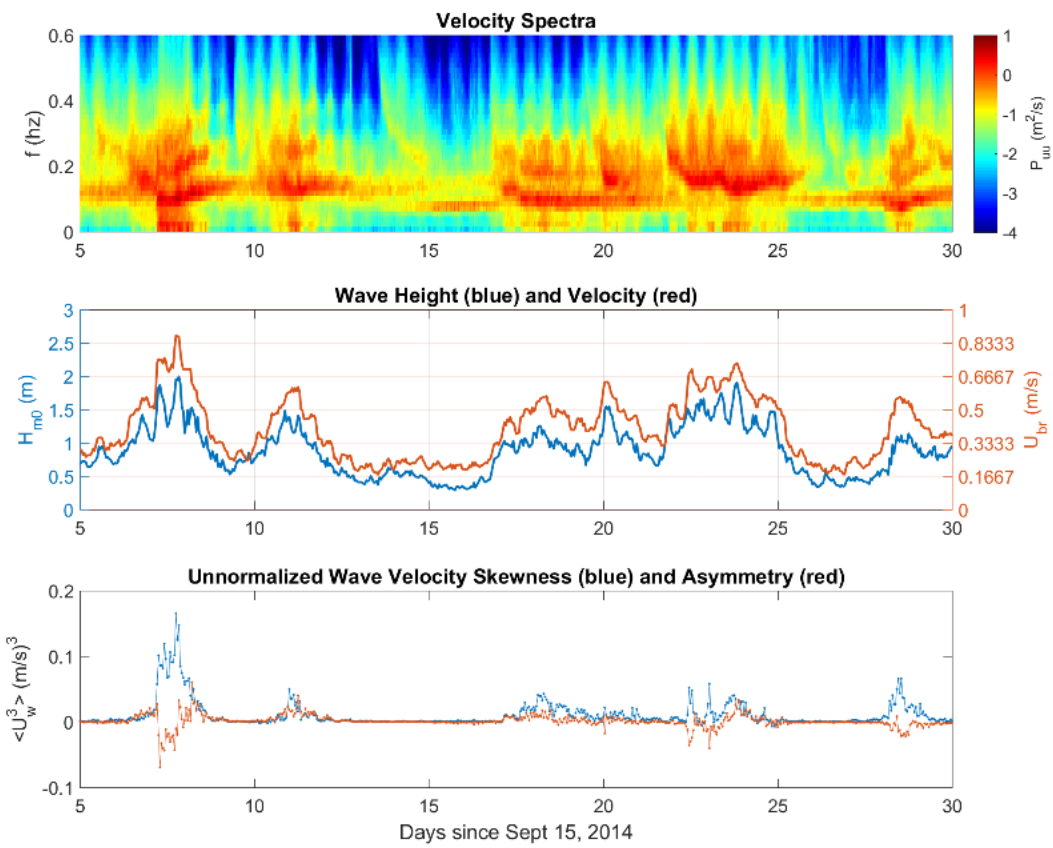

Figure 26. Time series of wave parameters at Long Point

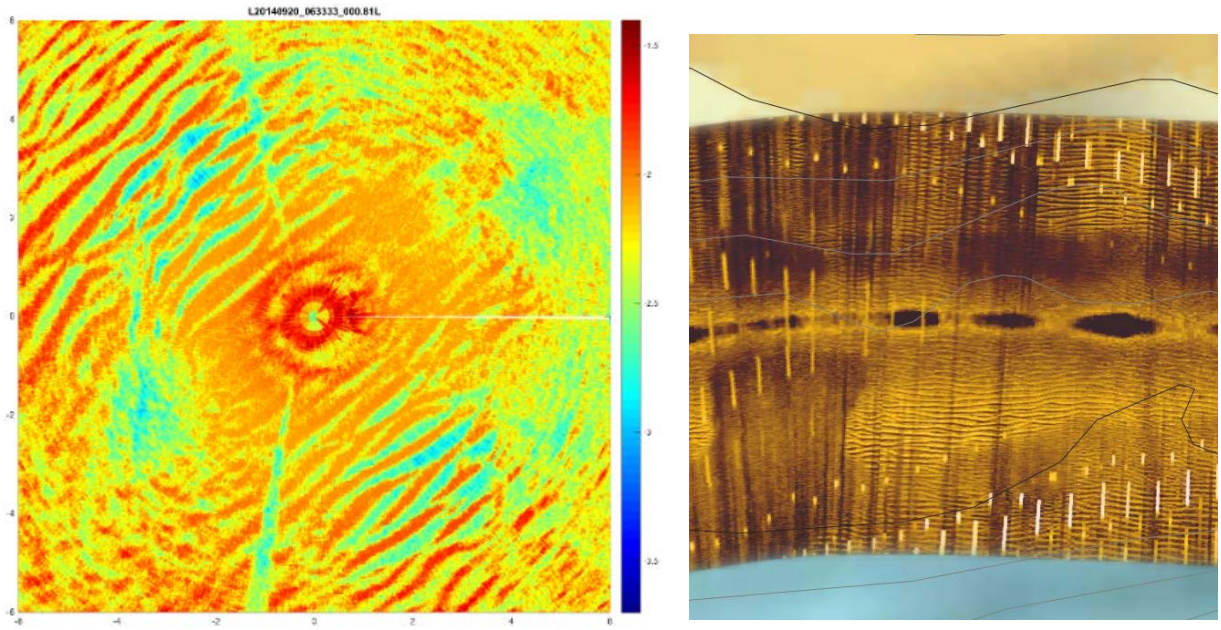

Figure 27. (a) Rotary sonar imagery and (b) Jetyak-based sidescan imagery of wave orbital scale ripples at Long Point

rip current feed into the hole in the bathymetry was often present at this location based on visual observations and drift trajectories while surveying.

The orbital velocity spectra from the pole-mounted sensor at the Long Point surf zone site look very different from the spectra at Wasque Shoals due to the depth-limited breaking in the surf zone (Figure 26). During high wave events, the waves show a harmonic structure with a primary peak at f = 0.1 Hz and harmonic peaks at 0.2 and 0.3 Hz. The harmonics adjust frequency coherently as the primary peak frequency shifts. The presence of the harmonics is indicative of shoaling and/or breaking waves in the surf zone that have high skewness and/or asymmetry. While the values of unnormalized and normalized skewness are 1.5 times higher ($\langle U_w^3 \rangle = 0.15, Sk = 0.7$) than those at Wasque Shoals ($\langle U_w^3 \rangle = 0.1, Sk =$0.4), the values of asymmetry are 5 times higher with $\langle H(U)_w^3 \rangle = -0.07$ as compared to –0.015 at Wasque. Negative asymmetry indicates forward-leaning waves. Interestingly, some wave events at the Long Point pole-mounted sensor have positive asymmetry. The combination of high skewness and asymmetry has the potential to force onshore migration of surrogate UXO.

4.2.2. Small-Scale Bedforms

In contrast to the large tidally forced mega-ripples at the Wasque Shoals site, the predominant type of bedform at Long Point in both Jetyak-based sidescan data and Quadpod-based rotary sidescan data are wave orbital scale ripples (Figure 27). These features have wavelengths (λ) that scale wave orbital diameter (d) with a typical scaling coefficient of 0.75 and a height that scales as 0.15 times the wavelength (24). In this case, the ripples had a wavelength of 0.75 cm. However, ripples in the surf zone are known to change geometry and type rapidly during storms (25), so these observations may only represent fair-weather conditions when we could perform sidescan surveys and before the quadpod broke free. During energetic breaking wave conditions, we expect a flat bed sheet flow in the surf zone. The lack of medium-scale bedforms at the Long Point site indicates there are fewer topographic barriers to UXO mobility compared to the large dunes and mega-ripples of Wasque Shoals. However, the bathymetry of nearshore sandbars is

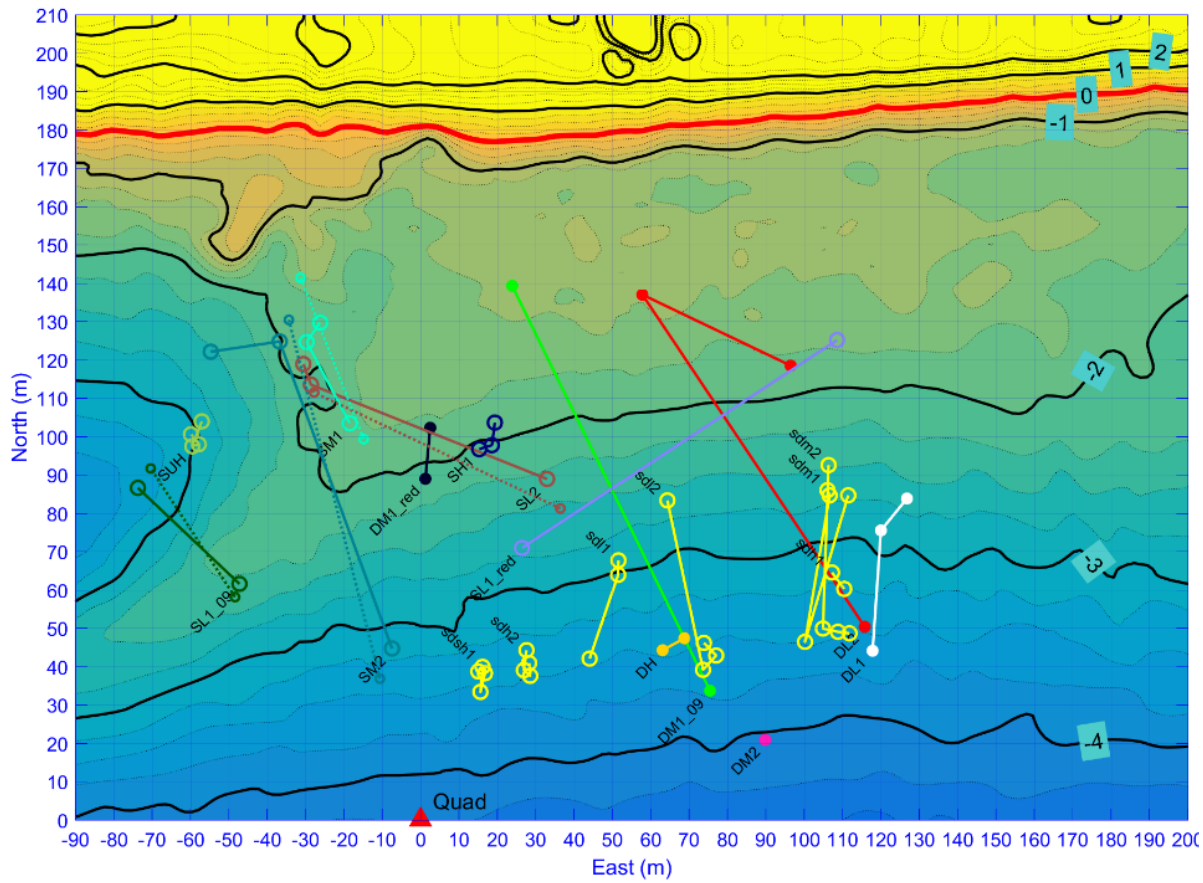

Figure 28. Bathymetry of Long Point surf zone and surrogate UXO trajectories

expected to have a first-order effect on cross-shore wave transformation and thus may control UXO mobility and the final location of UXO in the surf zone. This will be examined in more detail via numerical modeling in Section 4.3.1.

4.2.3. UXO Surrogate Deployments

4.2.3.1. Surrogate Mobility

UXO surrogate mobility was measured at the Long Point surf zone site using a combination of USBL transponder tracking and manual (swimming or small boat) GPS survey of the small floats attached to the surrogates. USBL range and bearing was only available on the S (shallow) series objects, while the D (deep) objects had range only. The s (small diameter) series were only tracked manually because they were too small to house USBL transponder electronics; S and D objects were also tracked manually, along with transponder tracking. The deployment location, intermediate manual track locations, and final recovery locations are shown in Figure 28 as solid lines with points at manually tracked locations. In addition, the locations of objects that were tracked with the USBL are shown as dashed lines with points at USBL-tracked locations. The USBL and manual track locations are usually within 10 m of each other, which could be explained by the scope of the buoy mooring lines. The USBL track points were averaged over the periods when the objects were not mobile. When the objects were mobile, the acoustic attenuation due to bubbles prevented USBL tracking (Figure 25) except at very close ranges.

In general, the lower density objects (L or M) migrated onshore, and the denser objects (H or UH) did not migrate and buried in place. The along-shore direction of migration was related to the directional spectra of the particular wave event in which the objects migrated. Most objects migrated primarily during the storm on days 7 through 9 with waves from the southeast. The

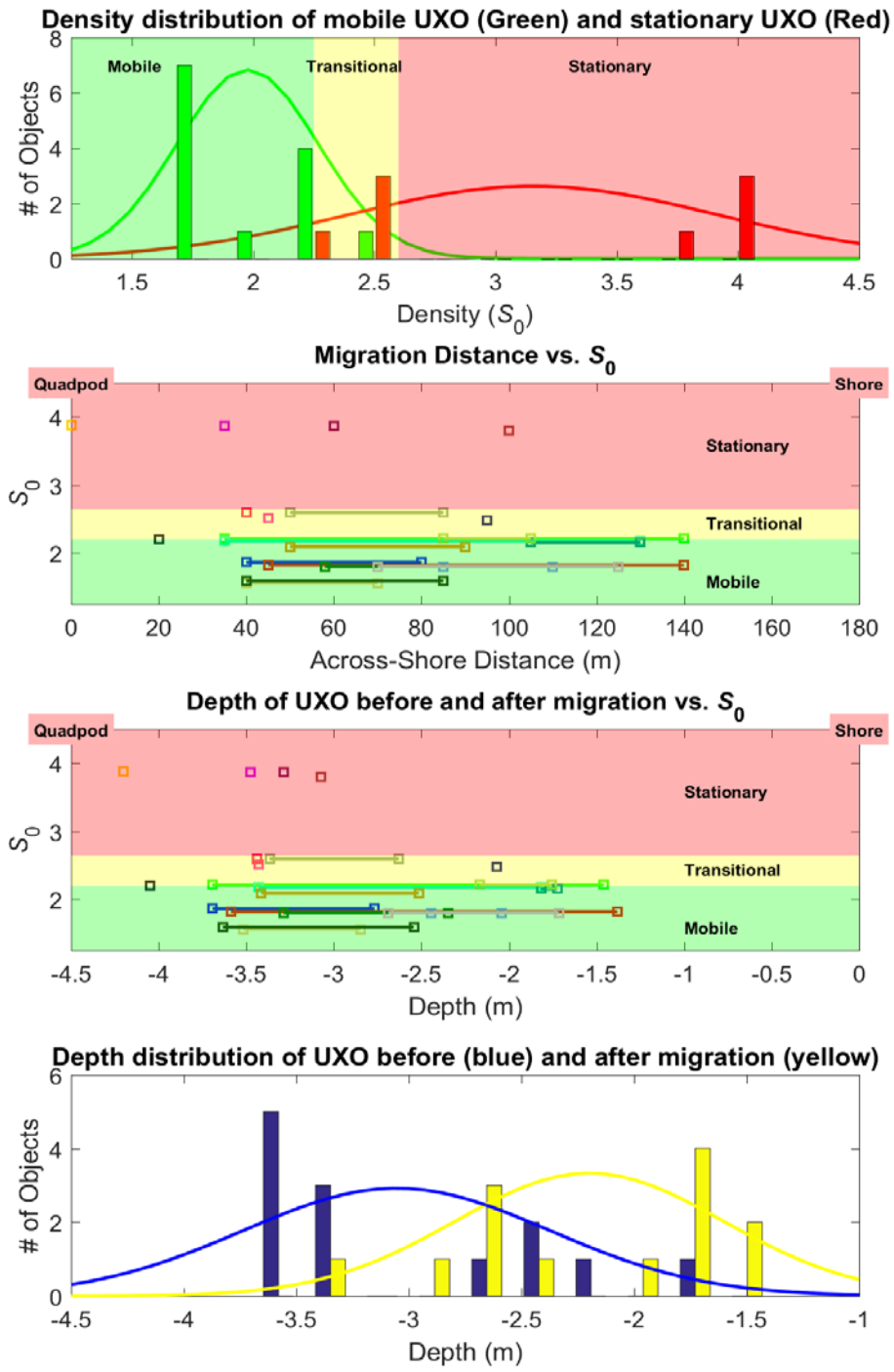

Figure 29. Distribution of stationary and mobile UXO vs. depth, density, and across-shore distance

most noticeable exception is object SL1_red (red for redeployed), which was recovered and redeployed on day 30 and migrated in response to waves from the southwest.

Figure 29 shows the density distribution of mobile and nonmobile UXO, the initial and final depths and cross-shore location as a function of object relative density (S_0), and the initial and final depth distribution of mobile UXO. The segregation of UXO objects into mobile and nonmobile classes was based on a threshold of migration distance ($\Delta X < 10$ m). Objects with S_0 less than 2.2 were always mobile; objects with S_0 between 2.2 and 2.65 were transitional, as some were mobile and others were not; and objects with S_0 greater than 2.65 were stationary.

For the mobile objects, migration distances varied from about 30 m to 100 m, with no objects ending closer than 40 m from the mid-tide (mean sea level) shoreline. This corresponds to a change in depth of the mobile objects beginning around 3.5 m and ending between 2.5 and 1.5 m. No objects migrated into water shallower than 1.3 m.

4.2.3.2. Surrogate Burial

Burial measurements were difficult to conduct due to the nature of scuba diving in the surf zone and the jet pump causing the objects to sink further into the liquefied sediment as we attempted to excavate the objects. The scuba divers performed rough estimates of the burial depth such as "at surface," "elbow deep," and "shoulder deep," and these were converted to quantitative burial depth based on the length of the individual scuba diver's arm.

Plotting relative burial against relative density shows there are no clear trends in this relationship (Figure 30). Most mobile objects eventually came to a final resting location and buried except for sdl2 and sdm2, which remained on the surface. Some stationary objects such as DH only buried to 15 cm. Most objects were eventually buried several object diameters below the surface with $b_d/D_0 > 1$. This variability is most likely due to the complexity of burial in the surf zone with mobile sandbars combined with scour and fill self-burial of the objects (3).

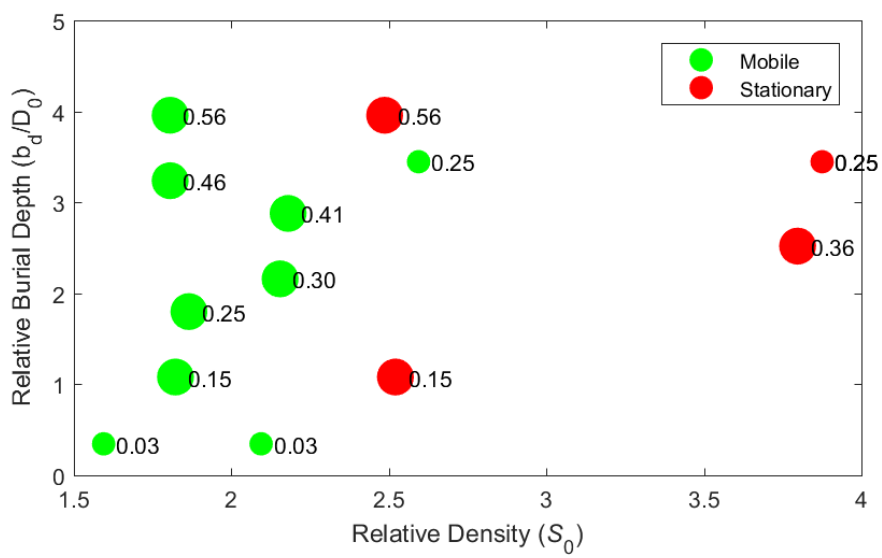

Figure 30. UXO relative burial depth vs. relative density (S_0) with physical burial depth (m) in text. Large symbols are D_0 = 14 cm objects, and small symbols are D_0 = 7 cm objects.

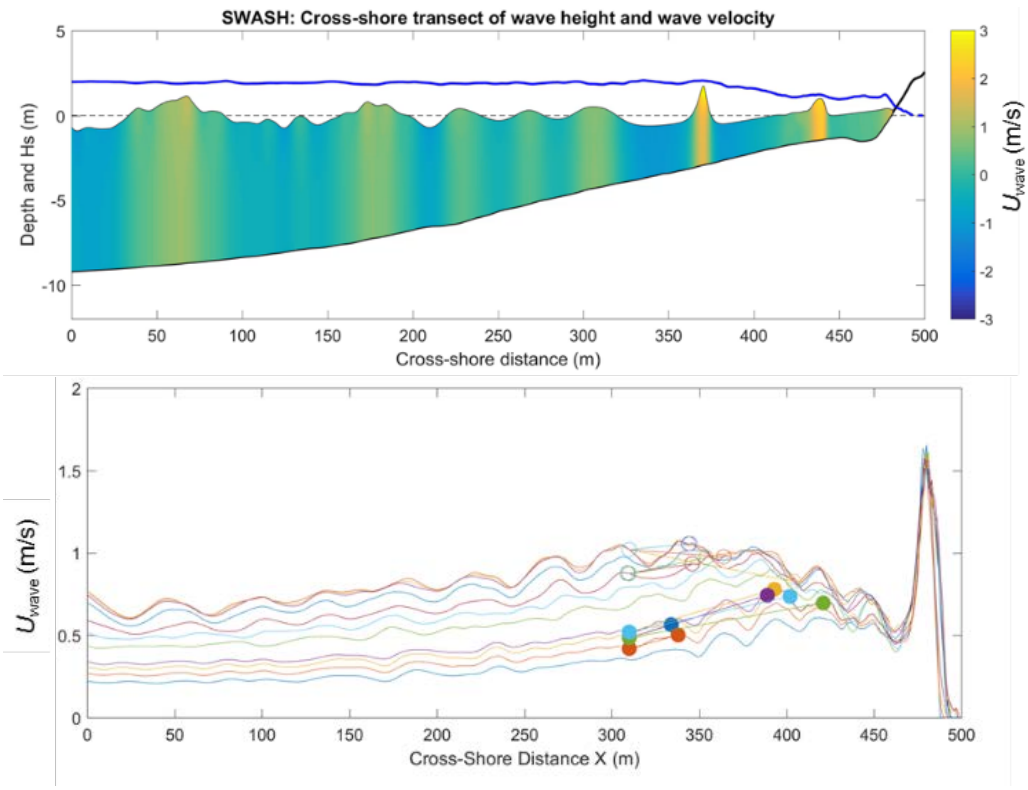

Figure 31. (a) Snapshot of SWASH output showing wave shoaling transformation, and (b) interpolation of wave orbital velocities from the sensor location to the UXO deployment location

4.3. **Discussion of Theory and Hydrodynamic Forcing**

4.3.1. Hydrodynamic Modeling

To determine thresholds for initiation of motion, hydrodynamic conditions at the UXO locations were required. In the surf zone, measurements taken at the quadpod or pole-mounted sensors could be quite different from conditions where the objects were deployed due to wave transformation and breaking. To relate hydrodynamic conditions at the location of the surrogate UXO to the conditions at the measurement sites, the Simulating WAves till SHore (SWASH) wave-resolving hydrodynamic model was used. This nonhydrostatic model resolves individual waves and has been shown in a variety of test cases to accurately capture nearshore wave transformation (26, 27). Here it is run in a 2D (across-shore and depth) resolving mode on a transect starting at 1 km offshore and ending at the crest of the beach dunes. The bathymetry/topography was extracted from a Jetyak bathymetry and GPS backpack beach topography survey through the middle of the deployment area. The model was initialized with wave spectra from the MVCO 12 m node at the offshore boundary condition for the first half (from background conditions to the peak wave height) of the wave event on days 2 to 4 (storm 1) and days 7 to 8 (storm 2). This provided 8 hourly runs for storm 1 and 11 hourly runs for storm 2. The results for storm 1 are shown in Figure 31. This data can be used to translate the wave orbital velocity measured at the sensors to the location of the UXO when motion was initiated.

The timing of the motion initiation of the UXO surrogates was determined from the r.m.s. variations of the roll of the surrogates as measured by the internal IMU sensors shown in Figure 32. A threshold of 10 degrees was used to determine the time that the object became mobile.

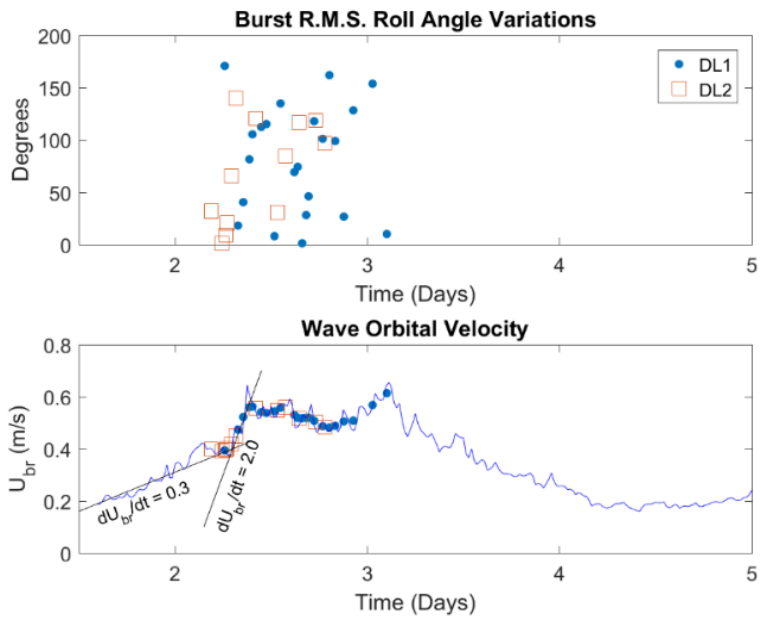

Figure 32. Time series of UXO r.m.s. roll variations and wave orbital velocity

Almost all IMU data bursts that exceeded the acceleration threshold to wake the data logger from its low-power sleep state had r.m.s. roll variations greater than 10 degrees. An example from objects DL1 and DL2 of time series data of burst r.m.s. roll variations and orbital velocity is shown in Figure 32. This time for initiation of motion was used to look up the wave orbital velocity (U_{br}) at the pole mount (storm 2) or quadpod (storm 1) at the same time.

The SWASH model results were then used to interpolate the measured U_{br} from the location of the hydrodynamic sensors to the location of the UXO. This interpolation generally resulted in an increase of U_{br} by a factor of approximately 1.5 as the objects were deployed offshore of the breakpoint (Figure 31). However, during the most energetic conditions, as the break point moved offshore, this interpolation resulted in a decrease in U_{br} at the shallower onshore UXO deployment locations. The SWASH output shows that wave orbital velocities decrease significantly in the last 50 m from the beach due to wave breaking offshore, before increasing again in the intermittently subaerial swash zone. This decrease in wave energy may explain why no objects migrated closer than 40 m from the shoreline.

4.3.2. Comparison to Parameterized Models

The initiation of motion data can be compared to parameterized theoretical models for initiation of motion (Eqn. 3) using the interpolated U_{br} from the measurements and the SWASH model. The initiation of motion model requires an initial state of burial, which was not known from the measurements, thus the model was run with 10% and 30% initial burial. The model predictions are shown as a curve of U_{br} for initiation of motion versus UXO relative density (S_o) (Figure 33(a)). Points above the curve are predicted to be mobile (green zone for p_b = 10%), and points below (red zone for p_b = 10%) are predicted to be stationary. The observations are plotted as green points in (U_{br}, S_o) space for mobile objects and red points for stationary objects. Both predictions for p_b of 10% and 30% are inconsistent with the observations of UXO mobility. A mobility threshold curve based on an initial state of burial of 10% incorrectly predicts that all objects, including those with S_o greater than 2.5, would be mobile. A threshold curve based on an

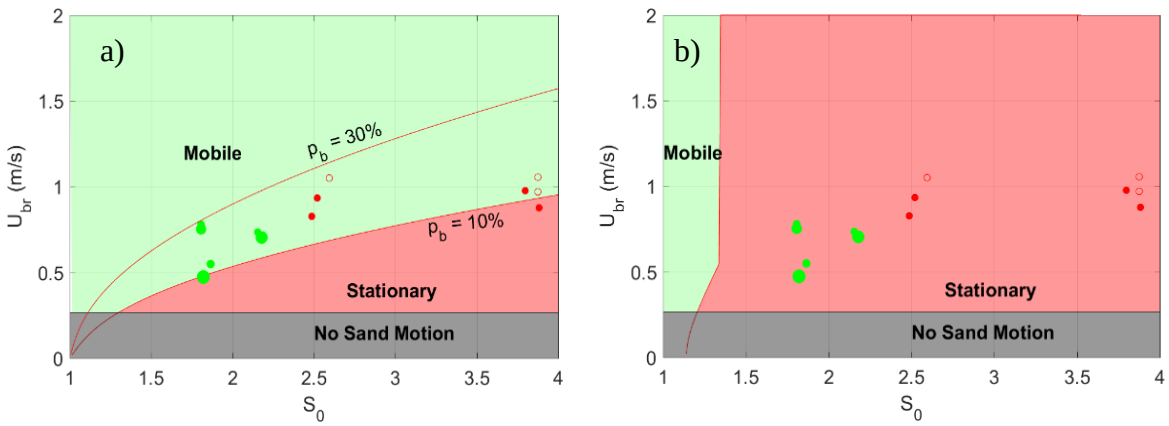

Figure 33 (a) Threshold for initiation of UXO motion as a function of U_{br} and S_o based on asumed initial burial of 10% and 30%. (b) Threshold for initiation of motion based on an equilibrium burial depth assumption.

initial state of burial of 30% incorrectly predicts that all objects, including those with S_o less than 2.5, would be stationary. Curves between 10% and 30% do not result in better predictions because the theory does not account for the dramatic change in mobility/burial behavior near a relative density of 2.2 to 2.6, which is slightly above the typical density of 2.0 for water-saturated sand beds.

4.3.2.1. Time-Dependent Burial Models

Because the burial process is known to be a time-dependent process, it is not physically realistic to assume a constant initial burial of some predetermined value. The threshold for mobility of objects on a mobile bed is likely to be set by the rate of burial relative to the rate of wave energy increase. If an initially proud object is instantaneously subjected to wave forcing greater than the threshold of motion, it will move before it has time to bury. If the wave forcing is increased very slowly with rates much slower than the timescale for burial, the object will become sufficiently buried with a burial depth given by the equilibrium burial depth (Eqn. 6), so it will not move unless the entire bed is fluidized, which requires extremely high wave energy. Mobility threshold predictions based on an assumption that an object is at its equilibrium burial depth are shown in Figure 33(b). This mobility threshold curve was determined by calculating an equilibrium burial depth for each combination of U_{br}, S_o and then calculating a threshold for mobility based on the equilibrium burial depth. At a value of U_{br} = 0.55 m/s, S_o = 1.4, the equilibrium burial depth was 50%, locking the object in place, so it was assumed that any points in the parameter's space with S_o > 1.4 would also be stationary. As intuitively expected, this curve incorrectly predicts that all objects in the measured data set would be buried.

A final set of calculations were performed by using the full time-dependent burial rate expression (Eqns. 6–9) with four different rates of wave energy increase (dU_{br}/dt). The waves were assumed to increase at a constant rate from an initial condition of a U_{br} determined by a 10% equilibrium burial, and Eqn. 7 was integrated in time to calculate a time-dependent burial depth. Using this burial depth and $U_{br}(t)$, a mobility threshold for S_o at each point in time was calculated based on Eqn. 3. Consistent with the equilibrium burial-based calculations, after an object was 50% buried, it was assumed the object would no longer be mobile, and any object with S_o greater than S_o for 50% burial would be locked in place. These time-dependent mobility curves show very different behavior than either the fixed burial depth curves or the equilibrium burial depth curves (Figure 34). Initially, when the waves are small, the mobility threshold curve follows the curve based on the initial burial of 10%. Depending on dU_{br}/dt, at some later time, the objects rapidly

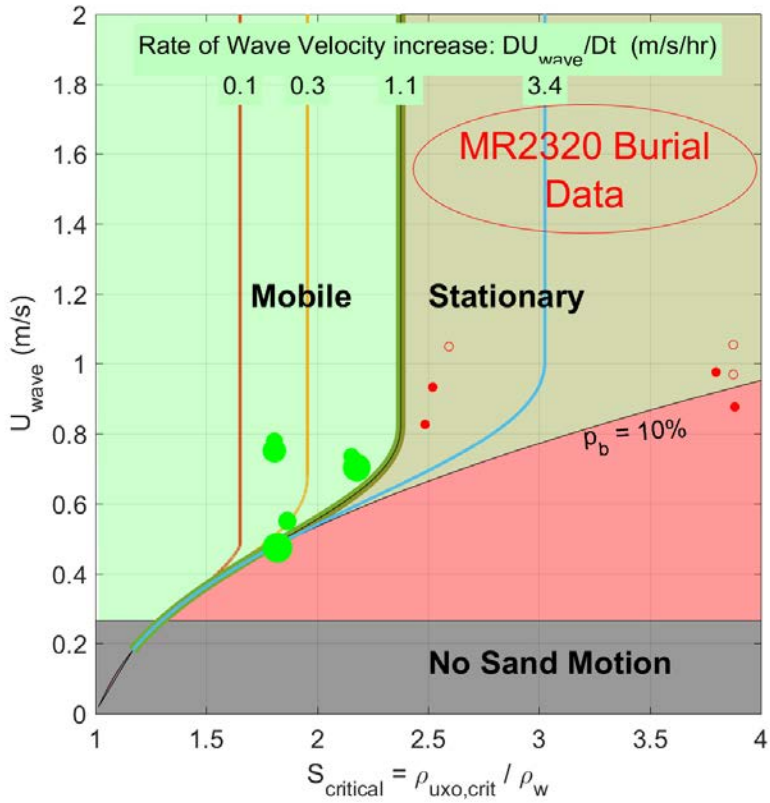

Figure 34. Threshold for initiation of UXO motion as a function of U_{br} and S_o based on a time-dependent burial fomulation with four different choices of the rate of wave velcoity change (dU_{br}/dt)

bury and are no longer mobile. For increasing values of dU_{br}/dt, this occurs at higher values of S_o. The curve for low values of dU_{br}/dt of 0.1 m/s/hr (10 hours to increase to 1 m/s waves) is consistent with the equilibrium burial mobility threshold curve in Figure 33(b). The curve for a high value of dU_{br}/dt of 3.4 m/s/hr indicates that even objects with S_o between 2.5 and 3.0 would be mobile with waves of U_{br} greater than 0.8 m/s. The measurements indicate that during the first storm of the deployment, the waves increased at a rate between $0.3 < dU_{br}/dt < 2.0$. The time-dependent mobility predictions with a $dU_{br}/dt = 1.1$ successfully segregates the data into mobile and stationary categories, roughly consistent with the data. To segregate the data successfully, the parameter M in the sediment transport rate formulation for the burial timescale (Eqn. 9) was increased from 0.11 to 0.5. If a value of 0.11 was used, objects with $S_o > 1.8$ would be predicted to be mobile at a high U_{br}. Increasing M from 0.11 to 0.5 increases the critical S_o from 1.8 to 2.2, consistent with the measurements.

5. Conclusions and Implications for Future Research/Implementation

The measurements and analysis of UXO surrogate mobility in this study span a range of conditions and object parameters in which high migration rates are possible. UXO surrogates with density above that of seawater but both below and above that of water-saturated sand, combined with energetic wave and current forcing, resulted in low migration distances in environments with bathymetric constraints and large migration distances in environments that were not bathymetrically constrained. In addition to wave forcing, the density of the objects

relative to the density of water-saturated sand appeared to play an important role in determining the threshold for mobility. Objects near to or less dense than water-saturated sand tended to migrate, and denser objects tended to bury.

Measurements of UXO mobility were conducted at a tidal shoals site that was also exposed to open ocean waves and a surf zone site that had weaker tidal currents. The bathymetry at the tidal shoals site was dominated by large migrating sand dunes with wavelengths of hundreds of meters and heights of 2 to 4 m. Despite energetic wave conditions, similar to those that caused large migration distances at the surf zone site, migration distances at the tidal shoals site were limited to a maximum of 14 m as the objects moved into the troughs of the large dunes. At the surf zone site, objects migrated from the outer surf zone 150 m across the surf zone to within 40 m of the beach, but no objects reached the beach. This is most likely due to the reduction of nearbed wave orbital velocities in the nearshore due to wave breaking further offshore.

Predictions of mobility based on parameterized force balances with a constant initial burial of 10% or 30% of the object diameter could *not* predict the measured transition from burial to mobility as a function of wave orbital velocity and UXO relative density. Calculations based on 10% initial burial incorrectly predicted that all objects in the measured data set would be mobile, and calculations based on 30% initial burial incorrectly predicted that all objects in the measured data set would be stationary. Time-dependent calculations, which account for the time required to bury an object, could successfully predict mobility transitions consistent with the observations. Although the time-dependent calculations are also able to predict the burial of objects, that is a separate study (MR-2320) conducted in more energetic conditions and higher relative densities, which would have been predicted to be mobile by calculations based on 10% to 30% initial burial (Figure 34). In these calculations, the timescale for burial is set by the ratio of the scour pit for the cross-sectional burial area relative to the sediment transport rate. If the waves increase quickly enough that an object does not have time to bury before the threshold for mobility is reached, it will migrate. If the waves increase slowly, these calculations predict that even low-density objects will bury. This time dependence of the relative roles of processes causing burial or mobility has important implications for both deterministic and statistical models for UXO mobility and burial. The time dependence also suggests that further observations would be useful to test the predictions shown in Figure 34. For instance, would rapidly increasing waves be able to mobilize objects with relative densities greater than 2.5?

In terms of object tracking methods, in energetic conditions, the GPS buoys were limited to use with only large objects due to the drag from the 10-cm diameter buoy required to float the GPS and batteries. The USBL tracking array and transponder system could track objects at the initial stages of mobility and could determine object locations before and after migration. Tracking was limited during periods of high mobility due to acoustic attenuation from bubbles. With the current design of the USBL transponder, this system was also limited to object diameters of 10 cm or larger. Future work should investigate the use of miniature low-power commercially available pingers for object localization systems. An additional important future technology development would be measurements of hydrodynamic forcing that moves with the mobile objects as conditions measured by fixed sensors are often quite different from conditions at the mobile objects in surf zone environments with high spatial variability.

6. Literature Cited

1. Protection, M.D.o.E. Martha's Vineyard - UXO Investigations. 2010; Available from: https://www.flickr.com/photos/massdep/5447757617/in/album-72157626055852190/.
2. Traykovski, P., et al. Mine Burial Experiments at the Martha's Vineyard Coastal Observatory. in Proceedings of the 6th International Symposium on Technology and the Mine Problem. 2004. Naval Postgraduate School, Monterey, California.
3. Traykovski, P., et al., Mine Burial Experiments at the Martha's Vineyard Coastal Observatory. Oceanic Engineering, IEEE Journal of, 2007. 32(1): p. 150-166.
4. Irish, J.D., et al., A self-contained sector-scanning sonar for bottom roughness observations as part of sediment transport studies. Journal of Atmospheric and Oceanic Technology, 1999. 16(11): p. 1830-1841.
5. Shields, A., Application of similarity principles and turbulence research to bed-load movement. 1936, Soil Conservation Service.
6. Rennie, S.E., A. Brandt, and C.T. Friedrichs, Initiation of motion and scour burial of objects underwater Ocean Engineering 2016(Submitted March, 2016).
7. Nielsen, P., Coastal bottom boundary layers and sediment transport. Vol. 4. 1992: World scientific.
8. Friedrichs, C.T., S.E. Rennie, and A. Brandt, Self-burial of objects on sandy beds by scour: A synthesis of observations, in Scour and Erosion, J. Harris and R. Whitehouse, Editors. 2016, CRC Press.
9. Catano-Lopera, Y.A. and M.H. García, Geometry of scour hole around, and the influence of the angle of attack on the burial of finite cylinders under combined flows. Ocean Engineering, 2007. 34(5): p. 856-869.
10. Whitehouse, R., Scour at marine structures: A manual for practical applications. 1998: Thomas Telford.
11. Traykovski, P., Observations of wave orbital scale ripples and a nonequilibrium time - dependent model. Journal of Geophysical Research: Oceans, 2007. 112(C6).
12. Meyer-Peter, E. and R. Müller. Formulas for bed-load transport. 1948. IAHR.
13. Demir, S.T. and M.H. García, Experimental studies on burial of finite-length cylinders under oscillatory flow. Journal of waterway, port, coastal, and ocean engineering, 2007. 133(2): p. 117-124.
14. Jenkins, S., G. D'Spain, and J. Wasyl, Vortex Lattice UXO Mobility Model for Reef-Type Range Environments. 2012, DTIC Document.
15. Jenkins, S.A., et al., Scour and burial mechanics of objects in the nearshore. Oceanic Engineering, IEEE Journal of, 2007. 32(1): p. 78-90.

16. Wilson, J.V., A. DeVisser, and B. Sugiyama, Predicting the Mobility and Burial of Underwater Unexploded Ordnance (UXO) Using the UXO Mobility Model (ESTCP) 200417. 2009, DTIC Document.

17. UXB International, I. Remedial Investigation Report, Tisbury Great Pond Investigation Area, Martha's Vineyard, Massachusetts. 2014; Available from: http://www.nae.usace.army.mil/Portals/74/docs/topics/MarthasVineyard/Tisbury/RemedialInvestigationReport.pdf.

18. Jaffré, F.M., et al. Ultra short baseline acoustic receiver/processor. in Europe Oceans 2005. 2005. IEEE.

19. Kimball, P., et al. The whoi jetyak: An autonomous surface vehicle for oceanographic research in shallow or dangerous waters. in 2014 IEEE/OES Autonomous Underwater Vehicles (AUV). 2014. IEEE.

20. Gonzalez-Rodriguez, D. and O.S. Madsen, Seabed shear stress and bedload transport due to asymmetric and skewed waves. Coastal Engineering, 2007. 54(12): p. 914-929.

21. Nielsen, P., Sheet flow sediment transport under waves with acceleration skewness and boundary layer streaming. Coastal Engineering, 2006. 53(9): p. 749-758.

22. Traykovski, P., Observations Of The Geometery And Migration Of Tidally Reversing Dunes, in The Proceedings of the Coastal Sediments 2015. 2015, World Scientific.

23. Samuelson, K. Migration of Multiple Scale Bedforms in Energetic Tidal Environments. in 2016 Ocean Sciences. 2016. New Orleans: AGU.

24. Traykovski, P., et al., Geometry, migration, and evolution of wave orbital ripples at LEO-15. Journal of Geophysical Research, C, Oceans, 1999. 104(1): p. 1505-1524.

25. Hay, A.E. and T. Mudge, Principal bed states during SandyDuck97: Occurrence, spectral anisotropy, and the bed state storm cycle. Journal of Geophysical Research: Oceans, 2005. 110(C3).

26. Zijlema, M., G. Stelling, and P. Smit, SWASH: An operational public domain code for simulating wave fields and rapidly varied flows in coastal waters. Coastal Engineering, 2011. 58(10): p. 992-1012.

27. Zijlema, M. Modelling wave transformation across a fringing reef using SWASH. in ICCE 2012: Proceedings of the 33rd International Conference on Coastal Engineering, Santander, Spain, 1-6 July 2012. 2012. Coastal Engineering Research Council.

7. Appendices

A. Supporting Data Table

a) Name	b) Diameter (m)	c) Mass (Kg)	d) Length (m)	e) Relative Density (S_o)	f) Migration Distance (m)	g) Start Depth (m)	h) End Depth (m)	i) Burial Depth (m)	j) Date Burial Depth	k) Quadpod Max Ubr (m/s)	l) Quadpod Max Object Shields	m) Quadpod Initial Motion Ubr (m/s)	n) UXO Initial Motion Ubr (m/s)
DL1	0.14	21.9	0.75	1.9	41	−3.7	−2.8	0.3	735900	0.65	0.36	0.47	0.55
DL2	0.14	21.4	0.75	1.8	112	−3.6	−1.4	0.2	735887	0.65	0.38	0.40	0.47
DM1	0.14	26.0	0.75	2.2	116	−3.7	−1.5	99.0	0	0.65	0.25		
DM2	0.14	25.9	0.75	2.2	0	−4.1	−4.1	999.0	0	0.90	0.49		
DH	0.14	29.6	0.75	2.5	0	−3.4	−3.4	0.2	735900	0.90	0.39		
DUH	0.14	45.6	0.75	3.9	0	−4.2	−4.2	99.0	0	0.90	0.20		
SL1	0.14	21.2	0.75	1.8	35	−2.3	−3.3	0.6	735900	0.90	0.73	0.52	0.78
SL2	0.14	21.2	0.75	1.8	70	−2.4	−2.0	0.5	735900	0.90	0.73	0.50	0.75
SUH	0.14	44.6	0.75	3.8	0	−3.1	−3.1	0.4	735900	1.06	0.29		
SM2	0.14	25.6	0.75	2.2	97	−3.4	−1.8	0.4	735900	0.90	0.50	0.50	0.70
SM1	0.14	25.3	0.75	2.2	32	−1.7	−1.8	0.3	735900	0.90	0.51	0.52	0.74
SH1	0.14	29.2	0.75	2.5	0	−2.1	−2.1	0.6	735900	1.06	0.54		
DM1rd	0.14	26.0	0.75	2.2	20	−2.2	−1.8	99.0	0	1.06	0.67		
SL1rd	0.14	21.2	0.75	1.8	101	−2.7	−1.7	99.0	0	1.06	1.01		
sdsh1	0.07	12.4	0.75	3.9	0	−3.5	−3.5	0.3	735900	1.06	0.54		
sdsh2	0.07	12.4	0.75	3.9	0	−3.3	−3.3	0.3	735900	0.90	0.39		
sdh2	0.07	8.3	0.75	2.6	0	−3.4	−3.4	99.0	0	1.06	0.97		
sdl1	0.07	5.0	0.75	1.6	30	−3.5	−2.8	99.0	0	0.73	1.32		
sdl2	0.07	5.1	0.75	1.6	46	−3.6	−2.5	0.03	735900	1.06	2.61		
sdm1	0.07	8.3	0.75	2.6	35	−3.4	−2.6	0.3	735900	0.73	0.47		
sdm2	0.07	6.7	0.75	2.1	40	-3.4	-2.5	0.03	735900	1.06	1.42		

Table 1a: Long Point surf zone object properties, migration, and burial statistics

a) Name	o) Start X Location (m)	p) Start Y Location (m)	q) End X Location (m)	r) End Y Location (m)	s) Start Deployment Date	t) End Deployment Date	u) Start Migration Date	v) End Migration Date
DL1	115	40	125	80	735858	735885	735859.3	735860.15
DL2	115	45	55	140	735858	735900	735859.3	735860.15
DM1	75	35	25	140	735858	735861	735859.4	735860.5
DM2	90	20	90	20	735858	735872	735858	735858
DH	60	45	60	45	735858	735872	735858	735858
DUH	0	0	0	0	735858	735872	735858	735858
SL1	–48	58	–70	85	735861	735885	735864.3	735867
SL2	35	85	–30	110	735861	735900	735864.2	735865.4
SUH	–60	100	–60	100	735861	735900	735858	735858
SM2	–10	35	–30	130	735861	735872	735864.2	735865.3
SM1	–10	105	–30	130	735861	735872	735863.4	735865.3
SH1	15	95	15	95	735872	735900	735858	735858
DM1rd	0	85	0	105	735887	735900	735887	735900
SL1rd	20	70	105	125	735887	735900	735887	735900
sdsh1	15	35	15	35	735876	735900	735858	735858
sdsh2	110	60	110	60	735876	735887	735858	735858
sdh2	30	40	30	40	735876	735900	735858	735858
sdl1	45	40	50	70	735876	735885	735876	735885
sdl2	75	40	65	85	735876	735900	735887	735900
sdm1	95	50	100	85	735876	735900	735876	735887

Table 1b: Long Point surf zone object properties, migration, and burial statistics (continued)

Notes on table data:

Tables 1a and 1b summarize the migration of UXO deployed at Long Point Beach, Martha's Vineyard. All dates are MATLAB serial date format, decimal days since 0/0/0 0:0:0.

a. Object Names are grouped by the following:

D series: Large diameter objects (with USBL/IMU sensors) deployed with a quadpod in slightly deeper water; L for light, M for Medium, H for heavy densities, UH for ultra-heavy.

S series: Large diameter objects (with USBL/IMU sensors) deployed with the pole-mounted USBL in slightly shallower water; L for light, M for Medium, H for heavy densities; rd indicates an object that was recovered during the deployment and redeployed.

sd: Small diameter objects.

b. Object Diameter (m)
c. Mass (Kg)
d. Length (m)
e. Relative Density ($S_o = \rho_o/\rho_w$)
f. Migration Distance (m), based on acoustic tracking or buoy GPS tracking

g. Start Depth (m), mean water depth at deployment
h. End Depth (m), mean water depth at recovery or end of migration for objects not recovered
i. Burial Depth (m), relative to seafloor. 0 = at the surface; 99 = buried and not recovered and known to have no motion due to tracking data or buried and recovered but no depth of burial measurements; 999 = not recovered and not known if occurred motion due to lack of tracking data.
j. Date Burial Depth, the date when burial measurements were conducted
k. Quadpod Max Ubr, measured at the quadpod or pole-mounted sensor; the maximum nearbed representative wave velocity (m/s) during the period of migration if the object migrated or during the whole deployment if no migration
l. UXO Max Object Shields, the object shields parameter (Eqn. 1) associated with Quadpod Max Ubr
m. Quadpod Initial Motion Ubr (m/s), the time of initiation of motion at the velocity sensor. The timing of the initiation of motion was determined from IMU data on the object.
n. UXO Initial Motion Ubr (m/s), the time of initiation of motion spatially translated to the UXO using the SWASH numerical wave transformation model (see Section 4.3.1)
o. Start x Location, at deployment, meters east from the quadpod
p. Start y Location, at deployment, meters north from the quadpod
q. End x Location, at recovery or end of migration, meters east from the quadpod
r. End y Location, at recovery or end of migration, meters north from the quadpod
s. Start Deployment Date, deployment or redeployment date
t. End Deployment Date, at recovery or not found during search
u. Start Migration Date, based on acoustic tracking or IMU data
v. End Migration Date, based on acoustic tracking or IMU data

Other data such as bathymetric data sets and hydrodynamic forcing time series are available from the lead investigator: ptraykovski@whoi.edu.

Technical Publications

a. Samuelson, K. *Migration of Multiple Scale Bedforms in Energetic Tidal Environments*. in *2016 Ocean Sciences*. 2016. New Orleans: AGU
b. Traykovski, P. *Phase lag control of tidally reversing mega-ripple geometry and bed stress in tidal inlets* in *2016 Ocean Sciences*. 2016. New Orleans: AGU
c. Traykovski, P. Observations of the Geometry and Migration of Tidally Reversing Dunes, Proceedings of Coastal Sediments, San Diego 2015